

Amortised Learning by Wake-Sleep

Li K. Wenliang¹ Theodore Moskovitz¹ Heishiro Kanagawa¹ Maneesh Sahani¹

Abstract

Models that employ latent variables to capture structure in observed data lie at the heart of many current unsupervised learning algorithms, but exact maximum-likelihood learning for powerful and flexible latent-variable models is almost always intractable. Thus, state-of-the-art approaches either abandon the maximum-likelihood framework entirely, or else rely on a variety of variational approximations to the posterior distribution over the latents. Here, we propose an alternative approach that we call amortised learning. Rather than computing an approximation to the posterior over latents, we use a wake-sleep Monte-Carlo strategy to learn a function that directly estimates the maximum-likelihood parameter updates. Amortised learning is possible whenever samples of latents and observations can be simulated from the generative model, treating the model as a “black box”. We demonstrate its effectiveness on a wide range of complex models, including those with latents that are discrete or supported on non-Euclidean spaces.

1. Introduction

Many problems in machine learning, particularly unsupervised learning, can be approached by fitting flexible parametric probabilistic models to data, often based on “local” latent variables whose number scales with the number of observations. Once the optimal parameters are found, the resulting model may be used to synthesise samples, detect outliers, or relate observations to a latent “representation”. The quality of all of these operations depends on the appropriateness of the model class chosen and the optimality of the identified parameters.

Although many fitting objectives have been explored in the literature, maximum-likelihood (ML) estimation remains

¹Gatsby Computational Neuroscience Unit. Correspondence to: Li K. Wenliang <kevinli@gatsby.ucl.ac.uk>.

prominent and comes with attractive theoretical properties, including consistency and asymptotic efficiency (Newey & McFadden, 1994). A challenge, however, is that analytic evaluation of the likelihoods of rich, flexible latent variable models is usually intractable. The Expectation-Maximisation (EM) algorithm (Dempster et al., 1977) offers one route to ML estimation in such circumstances, but it in turn requires an explicit calculation of (expected values under) the posterior distribution over latent variables, which also proves to be intractable in most cases of interest. Consequently, state-of-the-art ML-related methods almost always rely on approximations, particularly in large-data settings.

Denote the joint distribution of a generative model as $p_{\theta}(z, x)$ where z is latent and x is observed, and θ is the vector of parameters. EM breaks the ML problem into an iteration of two sub-problems. Given parameters θ_t on the t th iteration, first find the posterior $p_{\theta_t}(z|x)$; then maximise a lower bound to the likelihood that depends on this posterior to obtain θ_{t+1} . This bound is tight when computed using the correct posterior, ensuring convergence to a local mode of the likelihood.

The intractability of $p_{\theta}(z|x)$ forces some combination of Monte-Carlo estimation and the use of a tractable parametric approximating family which we call $q(z|x)$ (Bishop, 2006). To avoid repeating the expensive optimisation in finding $q(z|x)$ for each x , amortised inference trains an encoding or recognition model, with parameters ϕ , to map from any x directly to an approximate posterior $q_{\phi}(z|x)$. Examples of amortised inference models include the Helmholtz machine (Dayan et al., 1995; Hinton et al., 1995) trained by the wake-sleep algorithm; and the variational auto-encoder (VAE) (Kingma & Welling, 2014; Rezende et al., 2014) trained using reparameterisation gradient methods. With considerable effort on improving variational inference (reviewed in (Zhang et al., 2018)), complex and flexible generative models have been trained on large, high-dimensional datasets.

However, approximate variational inference poses at least three challenges. First, the parametric form of the approximate posterior $q(z|x)$, and particularly any factorisations assumed, must be crafted for each model. Second, methods such as reparameterisation require specific transformations tailored to the type of latent variables, whether they are continuous or discrete, and whether or not the support is

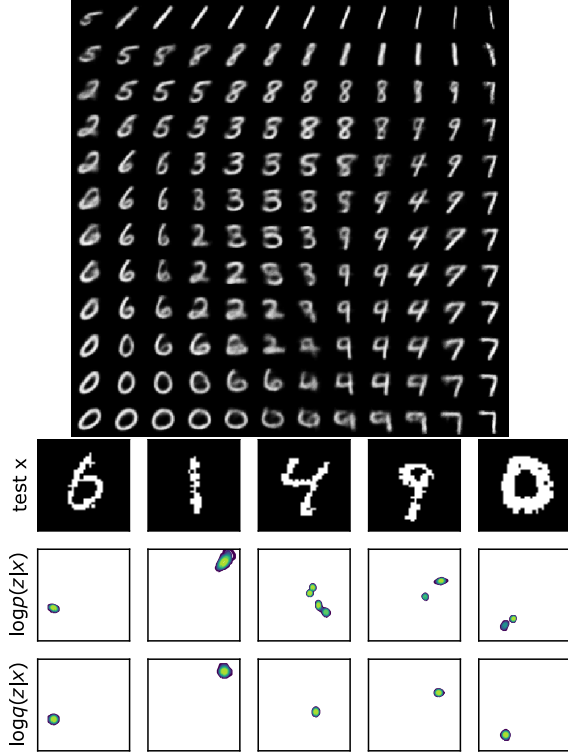


Figure 1. VAE trained on binarised MNIST digits. Top: mean images generated by decoding points on a grid of 2-D latent variables. Bottom three rows show five samples of real MNSIT digit (top), the corresponding true posteriors (middle) found by histogram and the approximate posteriors computed by the encoder.

Euclidean. Third, given a flexible generative model, such as one with conditional dependence modelled using neural networks, the true posteriors may be irregular in ways that are difficult to approximate. We illustrate this latter effect using a standard VAE with two-dimensional z trained on binarised MNIST digits (Figure 1). The exact posterior may be distorted or multi-modal, even though only Gaussian posteriors are ever produced by the encoder.

When inference is only approximate, the M-step of EM may not increase the likelihood, and so approximate methods usually converge away from the ML parameter values. The dependence of learnt parameters on the quality of the posterior approximation is not straightforward, and the error may not be reduced by (say) approximations with lower Kullback-Leibler (KL) divergence (Turner & Sahani, 2011); indeed errors in posterior statistics that enter the objective function may be unbounded (Huggins et al., 2019).

Here, we propose a novel approach to ML learning in flexible latent variable models that avoids the complications of posterior estimation, instead learning to predict the gradient of the likelihood directly—an approach we call *amortised learning*. The particular realisation we develop here, amor-

tised learning by wake sleep (ALWS), requires only that sampling from the generative model $p_{\theta}(z, x)$ be possible, and that the gradient $\nabla_{\theta} \log p_{\theta}(z, x)$ be available (possibly by automated methods), but otherwise does not make assumptions about the latent variable form or distribution. We test the performance of ALWS on a wide range of tasks and models, including hierarchical models with heterogeneous priors, nonlinear dynamical systems, and deep models of images. All experiments use the same form of gradient model trained by simple least-squares regression. For image generation, we find that models trained with ALWS can produce samples of considerably better quality than those trained using algorithms based on variational inference.

2. Background

2.1. Model Definition

Consider a probabilistic generative model with parameter vector θ that defines a prior on latents $p_{\theta}(z)$ and a conditional on observations $p_{\theta}(x|z)$. In ML learning, we seek parameters that maximise the log (marginal) likelihood

$$\log p_{\theta}(x) = \log \int p_{\theta}(z) p_{\theta}(x|z) dz \quad (1)$$

averaged over a set of i.i.d. data $\mathcal{D} = \{x_m^*\}_{m=1}^M$. One approach is to iteratively update θ by following the gradient

$$\Delta_{\theta}(x) := \nabla_{\theta} \log p_{\theta}(x) \quad (2)$$

at each iteration¹

2.2. Variational Inference for Learning

For many models of interest, the integral in (1) cannot be evaluated analytically, and so direct computation of the gradient is intractable. A popular alternative is to maximise a variational lower bound on the marginal likelihood defined by a distribution $q(z)$:

$$\mathcal{F}(q, \theta) := \mathbb{E}_{q(z)}[\log p_{\theta}(z, x)] + \mathbb{H}[q] \leq \log p_{\theta}(x), \quad (3)$$

where $\mathbb{H}[q]$ is the entropy of q . Thus, the parameter θ can be updated by following the gradient of $\mathcal{F}(q, \theta)$ w.r.t. θ

$$\begin{aligned} \nabla_{\theta} \mathcal{F}(q, \theta) &= \nabla_{\theta} \mathbb{E}_{q(z)}[\log p_{\theta}(z, x)] \\ &= \mathbb{E}_{q(z)}[\nabla_{\theta} \log p_{\theta}(z, x)]. \end{aligned} \quad (4)$$

When $q(z) = p_{\theta}(z|x)$, the lower bound in (3) is tight, and the gradient in (4) is equal to that of the likelihood (see Appendix A.3). Variational approximations attempt to bring q close to $p_{\theta}(z|x)$, usually by seeking to minimise $D_{\text{KL}}[q(z)||p_{\theta}(z|x)]$ (which corresponds to maximising the bound \mathcal{F} w.r.t. q). However, although minimising

¹We define the likelihood gradient for a single data point here and throughout; an actual update will typically follow the gradient averaged over i.i.d data.

$D_{\text{KL}}[q(z)||p_{\theta}(z|x)]$ over q ensures consistent optimisation of a single objective, the resulting gradient in (4) will often be a poor approximation to the likelihood gradient (2).

2.3. Conditional Expectation and LSR

Our approach is to avoid the difficulties introduced by approximating $p_{\theta}(z|x)$ with $q(z)$ in (4), and instead estimate the conditional expectation directly using least-squares regression (LSR). Let \mathbf{x} and \mathbf{y} be random vectors with a joint distribution $\rho(\mathbf{x}, \mathbf{y})$ on $\mathbb{R}^{d_x} \times \mathbb{R}^{d_y}$. In LSR, we seek a (vector-valued) function \mathbf{f} that achieves the lowest mean squared error (MSE) $\mathbb{E}_{\rho(\mathbf{x}, \mathbf{y})}[\|\mathbf{y} - \mathbf{f}(\mathbf{x})\|_2^2]$. The ideal solution is given by $\mathbf{f}_{\rho}(\mathbf{x}) := \mathbb{E}_{\rho(\mathbf{y}|\mathbf{x})}[\mathbf{y}]$, as the problem can be cast as the minimisation of $\mathbb{E}_{\rho(\mathbf{x})}[\|\mathbf{f}_{\rho}(\mathbf{x}) - \mathbf{f}(\mathbf{x})\|_2^2]$, where $\rho(\mathbf{x})$ is the marginal distribution of \mathbf{x} (see Appendix A.1). Note that $\mathbf{f}_{\rho}(\mathbf{x})$ takes a similar form as the desired (4). In practice, the distribution $\rho(\mathbf{x}, \mathbf{y})$ is known only through a sample $\{(\mathbf{x}_n, \mathbf{y}_n)\}_{n=1}^N \stackrel{\text{i.i.d.}}{\sim} \rho(\mathbf{x}, \mathbf{y})$; thus, LSR can be understood to seek a good approximation of \mathbf{f}_{ρ} based on the sample.

2.4. Kernel Ridge Regression

In LSR, as the target \mathbf{f}_{ρ} is unknown, it is desirable to construct an estimate without imposing restrictions on its form. Kernel ridge regression (KRR) is a nonlinear regression method that draws the estimated regression function from a flexible class of functions called a reproducing-kernel Hilbert space (RKHS) (Hofmann et al., 2008). The KRR estimator is found by minimising the regularised empirical risk

$$\min_{\mathbf{f} \in \mathcal{H}} \frac{1}{N} \sum_{n=1}^N \|\mathbf{y}_n - \mathbf{f}(\mathbf{x}_n)\|_2^2 + \lambda \|\mathbf{f}\|_{\mathcal{H}}^2, \quad (5)$$

where $\lambda > 0$ is a regularisation parameter, and \mathcal{H} is the RKHS corresponding to a matrix-valued kernel $\kappa : \mathbb{R}^{d_x} \times \mathbb{R}^{d_x} \rightarrow \mathbb{R}^{d_y \times d_y}$ (Carmeli et al., 2006). The solution can be found conveniently in closed-form, which allows a further simplification detailed in Section 3.2. In this paper, we use a kernel of the form $\kappa(\mathbf{x}, \mathbf{x}') = k(\mathbf{x}, \mathbf{x}')\mathbf{I}_y$, where \mathbf{I}_y is the identity matrix, and k is a scalar-valued positive definite kernel; therefore, the matrix-valued kernel κ can be identified with its scalar counterpart k . In particular, in the scalar output case $d_y = 1$, this choice of κ coincides with KRR with the scalar kernel k . Importantly, the closed-form solution $\hat{\mathbf{f}}_{\lambda}$ of KRR in (5) can be expressed as

$$\hat{\mathbf{f}}_{\lambda}(\mathbf{x}^*) = \mathbf{Y}(\mathbf{K} + N\lambda\mathbf{I}_N)^{-1}\mathbf{k}^*, \quad (6)$$

where \mathbf{Y} is the concatenation of the training targets $[\mathbf{y}_1, \dots, \mathbf{y}_N] \in \mathbb{R}^{d_y \times N}$, $\mathbf{K} \in \mathbb{R}^{N \times N}$ is the gram matrix whose element is $(\mathbf{K})_{ij} = k(\mathbf{x}_i, \mathbf{x}_j)$, \mathbf{I}_N is the identity matrix and $\mathbf{k}^* = (k(\mathbf{x}_i, \mathbf{x}^*))_{i=1}^N \in \mathbb{R}^N$ for a test point \mathbf{x}^* .

In the limit of $N \rightarrow \infty$ and $\lambda \rightarrow 0$, the solution $\hat{\mathbf{f}}_{\lambda}$ will

achieve the minimum MSE in the RKHS (Caponnetto & De Vito, 2007). In general, the target \mathbf{f}_{ρ} may not be in the RKHS²; nonetheless, if the RKHS is sufficiently rich (or C_0 universal (Carmeli et al., 2010)), the error made by the estimator $\mathbb{E}_{\rho(\mathbf{x})}[\|\hat{\mathbf{f}}_{\lambda}(\mathbf{x}) - \mathbf{f}_{\rho}(\mathbf{x})\|_2^2]$ will converge to zero (Szabó et al., 2016, Theorem 7).

3. Amortised Learning by Wake-Sleep

3.1. Gradient of Log-Likelihood

As stated above and derived in Appendix A.3, the log-likelihood gradient function evaluated on observation \mathbf{x} at iteration t (with current parameters θ_t) can be written

$$\begin{aligned} \Delta_{\theta_t}(\mathbf{x}) &= \nabla_{\theta} \log p_{\theta_t}(\mathbf{x})|_{\theta_t} \\ &= \nabla_{\theta} \mathcal{F}(p_{\theta_t}(\mathbf{z}|\mathbf{x}), \theta)|_{\theta_t}, \end{aligned} \quad (7)$$

where the gradient in the second line is taken w.r.t. the second argument of \mathcal{F} ; the posterior distribution is for a fixed θ at the current θ_t .

We want to directly estimate of this gradient without explicit computation of the posterior. Inserting the definition from (4) into (7) we have,

$$\Delta_{\theta_t}(\mathbf{x}) = \mathbb{E}_{p_{\theta_t}(\mathbf{z}|\mathbf{x})} [\nabla_{\theta} \log p_{\theta}(\mathbf{z}, \mathbf{x})|_{\theta_t}] \quad (8)$$

$$\begin{aligned} &= \nabla_{\theta} \mathbb{E}_{p_{\theta_t}(\mathbf{z}|\mathbf{x})} [\log p_{\theta}(\mathbf{z}, \mathbf{x})]|_{\theta_t} \\ &= \nabla_{\theta} J_{\theta}(\mathbf{x})|_{\theta_t}. \end{aligned} \quad (9)$$

where $J_{\theta}(\mathbf{x}) := \mathbb{E}_{p_{\theta_t}(\mathbf{z}|\mathbf{x})} [\log p_{\theta}(\mathbf{z}, \mathbf{x})]$. Note that the function $J_{\theta}(\mathbf{x})$ changes with iteration due to the dependence on $p_{\theta_t}(\mathbf{z}|\mathbf{x})$. It can be regarded as an instantaneous objective for ML learning starting from θ_t . Neither (8) nor (9) can be computed in closed form, and therefore need to be estimated. We refer to ML learning via the estimation of $\Delta_{\theta_t}(\mathbf{x})$ either through J_{θ} by (9) or directly by (8) as amortised learning. The difference between the two equations lies purely in implementation: The former estimates the high-dimensional $\Delta_{\theta_t}(\mathbf{x})$ directly, whereas the latter implements the same computation by differentiating $J_{\theta}(\mathbf{x})$. We term an estimator of J_{θ} a *gradient model*, as it retains information about θ and is used to estimate the gradient $\Delta_{\theta_t}(\mathbf{x})$. In the next section, we develop a concrete instantiation of amortised learning.

3.2. Training KRR Gradient Model by Wake-Sleep

As discussed in Section 2.3, LSR allows us to estimate the conditional expectation of an output variable given an input. Thus, although the gradient in (8) (or in (9)) involves an intractable conditional expectation, we can obtain an estimate of the gradient $\Delta_{\theta_t}(\mathbf{x})$ by regressing from \mathbf{x} to

²In this case, \mathbf{f}_{ρ} is only assumed to be square-integrable with respect to ρ

$\nabla_{\theta} \log p_{\theta}(z, x)$ (or $\log p_{\theta}(z, x)$). Any reasonable regression model, e.g., a neural network, could serve this purpose, but here we choose to use KRR introduced in Section 2.4. Other possible forms of gradient model are discussed in Appendix B.1.

The expression in (8) leads to the following LSR problem

$$\min_{f \in \mathcal{H}} \frac{1}{N} \sum_{n=1}^N \|\nabla_{\theta}(y_{\theta,n})|_{\theta_t} - f(x_n)\|_2^2 + \lambda \|f\|_{\mathcal{H}}^2, \quad (10)$$

where $y_{\theta,n} = \log p_{\theta}(z_n, x_n)$, $\tilde{\mathcal{H}}$ is an RKHS and $\{(z_n, x_n)\}_{n=1}^N \sim p_{\theta_t}$. Brehmer et al. (2020) also noticed that log-likelihood gradient could be obtained by LSR. However, regressing to a vector-valued $\nabla_{\theta} \log p_{\theta}$ can be expensive, and evaluating the target $y_{\theta,n}$ on all (z_n, x_n) is slow. Alternatively, we can use (9) and find an estimator for the scalar-valued J_{θ} that keeps the dependence on θ and then evaluate its gradient by automatic differentiation. Thus, we construct an estimator by

$$\hat{J}_{\theta,\gamma} = \arg \min_{f \in \mathcal{H}} \frac{1}{N} \sum_{n=1}^N |y_{\theta,n} - f(x_n)|^2 + \lambda \|f\|_{\mathcal{H}}^2, \quad (11)$$

where \mathcal{H} is the RKHS induced by a kernel $k_{\omega}(\cdot, \cdot)$ with hyperparameters ω , and $\gamma = \{\omega, \lambda\}$. For each data point $x^* \in \mathcal{D}$, the estimate of $J_{\theta}(x^*)$ is

$$\hat{J}_{\theta,\gamma}(x^*) = \alpha_{\theta,\gamma} \cdot k_{\omega}^*, \quad (12)$$

$$\alpha_{\theta,\gamma} = y_{\theta} (K_{\omega} + \lambda N I_N)^{-1}, \quad (y_{\theta})_n = \log p_{\theta}(z_n, x_n) \\ K_{\omega,i,j} = k_{\omega}(x_i, x_j), \quad k_{\omega}^* = k_{\omega}(x_j, x^*)$$

where I_N is the identity matrix of size $N \times N$. Note that the dependence of $\hat{J}_{\theta,\gamma}$ on θ is only through evaluations of $\log p_{\theta}(z, x)$ on samples drawn from p_{θ_t} for fixed $\theta = \theta_t$. The gradient $\Delta_{\theta_t}(x)$ is then estimated as

$$\hat{\Delta}_{\theta_t,\gamma}(x) := \nabla_{\theta} \hat{J}_{\theta,\gamma}(x)|_{\theta_t}.$$

In general, a good estimator of J_{θ} may not yield a reliable estimate of its gradient $\nabla_{\theta} J_{\theta}$; however, for the KRR estimate, taking the derivative of $\hat{J}_{\theta,\gamma}$ w.r.t. θ is equivalent to replacing y_{θ} in (12) with $\nabla_{\theta}(y_{\theta})|_{\theta_t}$, which is the solution for the optimisation in (10), with \mathcal{H} being a vector-valued RKHS given by a kernel $\kappa_{\omega} = k_{\omega}I$ (see Section 2.4). We show in Appendix A.2 that, under mild conditions, the target of the regression $\mathbb{E}_{p_{\theta_t}(z|x)} [\nabla_{\theta} y_{\theta,n}|_{\theta_t}]$ is square-integrable under $p_{\theta_t}(x)$ for common generative models.

In summary, learning proceeds according to the following wake-sleep procedure: at the t th step when $\theta = \theta_t$, the gradient model is first trained using “sleep samples” $(z_n, x_n) \sim p_{\theta_t}$ and evaluations $\log p_{\theta}(z_n, x_n)$, keeping the dependence on θ ; then the gradient model is applied to real data (“wake” samples) $x^* \in \mathcal{D}$ to produce $\hat{\Delta}_{\theta_t,\gamma}(x^*)$ by

differentiating $\hat{J}_{\theta,\gamma}$ and evaluating at θ_t . See Algorithm 1. Two points are worth emphasis: (a) The algorithm does not require explicit computation or approximation of the posterior, and (b) We only need samples from the model $p_{\theta}(z, x)$ and differentiable evaluations of $\log p_{\theta}(z, x)$.

3.3. Exponential Family Conditionals

In many common models, the conditional $p_{\theta}(x|z)$ lies in the exponential family (e.g. Gaussian, Bernoulli), and we can exploit this structure to simplify the estimation of J_{θ} . In this case, the log joint can be written as

$$\begin{aligned} \log p_{\theta}(z, x) &= \log p_{\theta}(x|z) + \log p_{\theta}(z) \\ &= \eta_{\theta}(z) \cdot s(x) - \log Z_{\theta}(z) + \log p_{\theta}(z) \\ &= \eta_{\theta}(z) \cdot s(x) - \Psi_{\theta}(z) \end{aligned}$$

where $\eta_{\theta}(z)$, $s(x)$ and $Z_{\theta}(z)$ are, respectively, the natural parameter, sufficient statistics and normaliser of the likelihood, and $\Psi_{\theta} := \log Z_{\theta}(z) - \log p_{\theta}(z)$. By taking the posterior expectation, $J_{\theta}(x)$ in (9) becomes

$$J_{\theta}(x) = \underbrace{\mathbb{E}_{p_{\theta_t}}[\eta_{\theta}(z)]}_{h_{\theta}^{\eta}(x)} \cdot s(x) - \underbrace{\mathbb{E}_{p_{\theta_t}}[\Psi_{\theta}(z)]}_{h_{\theta}^{\Psi}(x)} \quad (13)$$

where p_{θ_t} stands for $p_{\theta_t}(z|x)$. Therefore, for exponential family likelihoods, the regression to $\log p_{\theta}(z, x)$ in (11) can be replaced by two separate regressions to $\eta_{\theta}(z)$ and $\Psi_{\theta}(z)$, which are functions of z alone. The resulting estimators $\hat{h}_{\theta,\gamma}^{\eta}$ and $\hat{h}_{\theta,\gamma}^{\Psi}$ are combined to yield

$$\hat{\Delta}_{\theta_t,\gamma}(x) = \nabla_{\theta} \left[\hat{h}_{\theta,\gamma}^{\eta}(x) \cdot s(x) \right] \Big|_{\theta_t} - \nabla_{\theta} \hat{h}_{\theta,\gamma}^{\Psi}(x) \Big|_{\theta_t},$$

where the Jacobian vector product applies to the first term.

3.4. Kernel Structure and Learning

The kernel k_{ω} used in the gradient model affects how well $\Delta_{\theta_t}(x)$ is estimated. It can be made more flexible by augmenting with a neural network as in (Wilson et al., 2016; Wenliang et al., 2019)

$$k_{\omega}(x, x') = \kappa_{\sigma}(\psi_v(x), \psi_v(x'))$$

where κ_{σ} is a standard kernel (e.g. exponentiated-quadratic) with parameter σ (e.g. bandwidth), and ψ_v is a neural network with parameter v , so $\omega = \{\sigma, v\}$. Other details of the kernel structure are described in Appendix B.2.

The gradient model parameter $\gamma = \{\omega, \lambda\}$ can be learned to further minimise the MSE in (11) using a scheme of cross-validation by gradient descent (Wenliang et al., 2019). Specifically, we generate two sets of sleep samples from p_{θ} ; we use one set to compute $\alpha_{\theta,\gamma}$ in closed form; then, on the other set $\{(z'_l, x'_l)\}_{l=1}^L$, we compute the MSE between the estimator $\hat{J}_{\theta,\gamma}(x'_l)$ and the ground truth value $\log p_{\theta}(z'_l, x'_l)$, and minimise this by gradient descent on γ . The full ALWS procedure is presented in Algorithm 1.

Algorithm 1: Amortised learning by wake sleep

input : Dataset \mathcal{D} , gradient model parameters γ ,
 generative model $\log p_\theta(\mathbf{z}, \mathbf{x})$, or η_θ and Ψ_θ
 with parameters θ initialised s.t. $p_\theta(\mathbf{x})$
 covers/dominates the data distribution, max
 epoch and any convergence criteria.

while θ not converged within max epoch **do**

Sleep phase: train gradient model

Sample $\{\mathbf{z}_n, \mathbf{x}_n\}_{n=1}^N \sim p_\theta$

if $p(\mathbf{x}|\mathbf{z})$ is not in exponential family **then**

Find $\hat{J}_{\theta, \gamma}(\cdot)$ by computing $\alpha_{\theta, \gamma}$ in (12)

else

Find $\hat{h}_{\theta, \gamma}^\eta(\cdot)$ and $\hat{h}_{\theta, \gamma}^\Psi(\cdot)$ similar to (12)

$\hat{J}_{\theta, \gamma}(\cdot) = \hat{h}_{\theta, \gamma}^\eta(\cdot) \cdot s(\mathbf{x}) - \hat{h}_{\theta, \gamma}^\Psi(\cdot)$ in (13)

Sleep phase: update γ

Sample $\{\mathbf{z}'_l, \mathbf{x}'_l\}_{l=1}^L \sim p_\theta$

Compute $d_l := \log p_\theta(\mathbf{z}, \mathbf{x})$

Compute $\mathcal{E}_\gamma = \frac{1}{L} \sum_{l=1}^L (\hat{J}_{\theta, \gamma}(\mathbf{x}'_l) - d_l)^2$

Update $\gamma \propto \nabla_\gamma \mathcal{E}_\gamma$

Wake phase: update θ

Sample $\{\mathbf{x}_m^*\}_{m=1}^M \in \mathcal{D}$

$\bar{J}_\theta = \frac{1}{M} \sum_i \hat{J}_{\theta, \gamma}(\mathbf{x}_m^*)$

Update $\theta \propto \nabla_\theta \bar{J}_\theta$

end

return : θ

3.5. Dealing with Covariate Shift

The gradient model is to be used to estimate $\Delta_{\theta_t}(\mathbf{x})$ on \mathbf{x}^* drawn from an underlying data distribution p^* , but it is trained using sleep samples from p_{θ_t} . This mismatch in input data distribution for training and evaluation is known as covariate shift (Shimodaira, 2000).

Here, to ensure that the gradient model performs reasonably well on p^* , we initialise $p_\theta(\mathbf{x})$ to be overdispersed relative to p^* by setting a large noise in $p_\theta(\mathbf{x}|\mathbf{z})$. Since ML estimation minimises $D_{\text{KL}}[p^*||p_\theta]$, which penalises a distribution p_θ that is narrower than p^* , we expect the noise to continue to cover the data before the model is well trained. For image data only, we also apply batch normalisation in ψ_w of the kernel. We find these simple remedies to be effective, though other more principled methods, such as kernel mean matching (Gretton et al., 2009) and binary classification (Gutmann & Hyvärinen, 2010; Goodfellow et al., 2014), may further improve the results.

4. Experiments

We evaluate ALWS on a wide range of generative models. Details for each experiment can be found in Appendix C.³

³Code is at github.com/kevin-w-li/al-ws

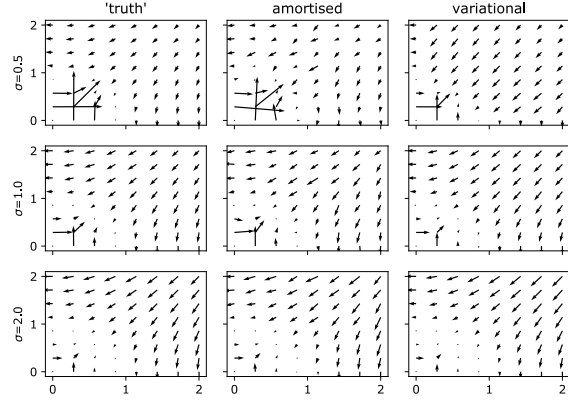


Figure 2. Gradient estimated using amortised learning and variational inference. The true gradients are approximated by importance sampling.

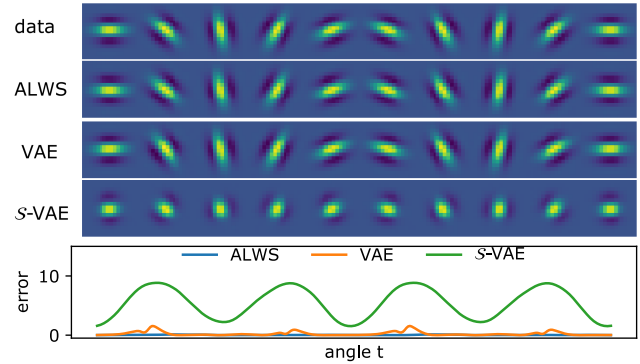


Figure 3. Learning to generate Gabor filters given a 1-D circular uniform prior. Top images show samples generated by latents separated by fixed rotation on the circle. For VAE, a 2-D Gaussian prior was used, and the images are generated by latents on the unit circle. S-VAEs cannot reliably learn the filters. The errors below show the squared distance between generated images and data at each orientation. For each method, an angle offset and direction are chosen to minimise the total error.

4.1. Parameter Gradient Estimation

First, we demonstrate that KRR can estimate $\Delta_{\theta_t}(\mathbf{x})$ well on a simple toy generative model described by

$$z_1, z_2 \sim \mathcal{N}(0, 1), \quad \mathbf{x}|\mathbf{z} \sim \mathcal{N}(\text{softplus}(\mathbf{b} \cdot \mathbf{z}) - \|\mathbf{b}\|_2^2, \sigma_x^2).$$

The training data are 100 data points from the model given $\mathbf{b} = [1, 1]$, $\sigma_x = 0.1$. We estimate the gradients of the log-likelihood w.r.t. \mathbf{b} evaluated at a grid of \mathbf{b} by ALWS, and compare them to estimates using importance sampling (“truth”) and a factorised Gaussian posterior that minimises the forward KL for each \mathbf{x} . For ALWS, we used a Gaussian kernel with a bandwidth equal to the median distance between samples generated for each \mathbf{b} , and set $\lambda = 0.01$. For variational inference, we assumed a factorised Gaussian posterior for each sample of \mathbf{x} , and optimise posterior pa-

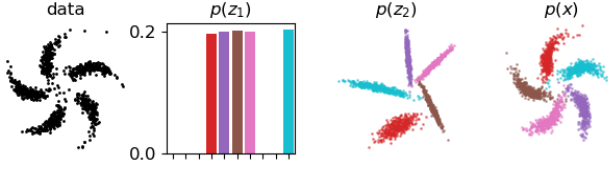


Figure 4. Learning hierarchical model with discrete and continuous latents. From left to right: data sample, component probabilities, samples of the first latent distribution and samples of generated data. Colours correspond to different components

rameters until convergence. ALWS tends to estimate better, especially for small b (Figure 2). For the smallest σ_x , the KRR estimates are noisier, whereas variational inference introduces greater bias.

4.2. Non-Euclidean Priors

The prior $p(z)$ may capture special topological structures in the data. For instance, a prior over the hypersphere can be used to describe circular features (Davidson et al., 2018; Xu & Durrett, 2018). Training models with such a prior is straightforward using ALWS, while learning by amortised inference requires special reparameterisation for a posterior on the hypersphere, such as the von-Mises Fisher (vMF) used in the \mathcal{S} -VAE (Davidson et al., 2018; Xu & Durrett, 2018). We fit a model with uniform circular latent and neural-network output:

$$z = [\cos(a), \sin(a)], \quad p(a) = \mathcal{U}(a; (-\pi, \pi)), \\ p(x|z) = \mathcal{N}(x; \text{NN}_w(z), \sigma_x^2 \mathbf{I}),$$

(where \mathcal{U} is a uniform distribution) on a data set of Gabor wavelets with uniformly distributed orientations. As shown in Figure 3, ALWS learns to generate images that closely resemble the training data. A fixed rotation around the latent circle corresponds to almost a fixed rotation of the Gabor wavelet in the image. The VAE with a 2-D Gaussian latent also generates good filters given latents on the circle, but the length of the filter varies with rotation. Surprisingly, \mathcal{S} -VAE is not able to learn on this dataset, the vMF posterior is almost flat for any input image. This hints at potential optimisation issues with the complicated reparameterisation. This advantage also extends to priors over the hyperbolic space, which are used to capture tree-like hierarchical structures (Nagano et al., 2019; Mathieu et al., 2019).

4.3. Hierarchical Models

Rich hierarchical structures in the data can be captured with multiple layers of latents. Provided that samples can be drawn from the hierarchical model and the joint log-likelihood evaluated, ALWS extends straightforwardly to hierarchies, even with mixed discrete and continuous latents. The pinwheel distribution (Johnson et al., 2016; Lin et al.,

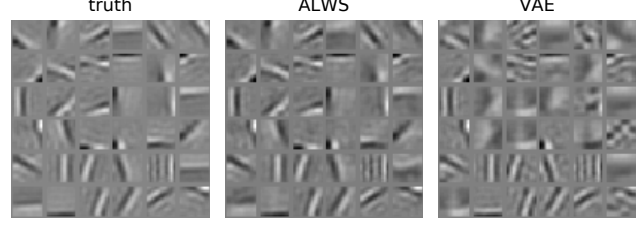


Figure 5. Feature identification. Left, true basis used to generate images. Middle, basis recovered by ALWS. Right, basis recovered by VAE. The filters are arranged according to correlations with the true basis.

2018) has five clusters of distorted Gaussian distributions (Figure 4), and can be described by the following model:

$$p(z_1) = \text{Cat}(z_1; \mathbf{m}), \quad p(z_2|z_1 = k) = \mathcal{N}(z_2; \mu_k, \Sigma_k), \\ p(x|z_2) = \mathcal{N}(x; \text{NN}_w(z_2), \Sigma_x),$$

where Cat is the categorical distribution. The parameters are the logits \mathbf{m} in 10 dimensions, the means and covariance matrices of the component distributions $\{\mu_k, \Sigma_k\}_{k=1}^{10}$, the weights \mathbf{w} in NN, and the diagonal covariance Σ_x . The logits \mathbf{m} are penalised according to a Dirichlet prior, and $\{\mu_k, \Sigma_k\}_{k=1}^{10}$ by a normal-Wishart prior. After training with ALWS, the categorical distribution correctly identifies the five components, and the generated samples match the training data. We compare these samples with those reconstructed from a Bayesian version of the model trained by structured inference network (SIN) (Lin et al., 2018)⁴. A three-way maximum mean discrepancy (MMD) test (Bou-liphone et al., 2016) finds that samples from the two models are equally close to the training data ($p = 0.514$, $N = 1,000$ samples). Details are in Appendix C.3.

4.4. Feature Identification

Independent Components. Learning informative features from complex data can benefit downstream tasks. We use ALWS to identify features from data generated by

$$p(z_i) = \text{Lap}(z_i; 0, 1), \quad p(x|z) = \mathcal{N}(x; \mathbf{W}z, \sigma^2 \mathbf{I}),$$

where Lap is the Laplace distribution, $\sigma = 0.1$ and basis \mathbf{W} contains independent components of natural images (Hateren & Schaaf, 1998) found by the FastICA algorithm (Hyvärinen & Oja, 2000). Since this model is identifiable, we perform model recovery from a random initialisation of \mathbf{W} using ALWS and compare with a VAE. ALWS clearly finds better features, as shown in Figure 5. On generated samples, a three-way MMD test favours ALWS over the Laplace-VAE ($p < 10^{-5}$) based on 10,000 samples. Details are in Appendix C.4.

⁴github.com/emtiyaz/vmp-for-svae

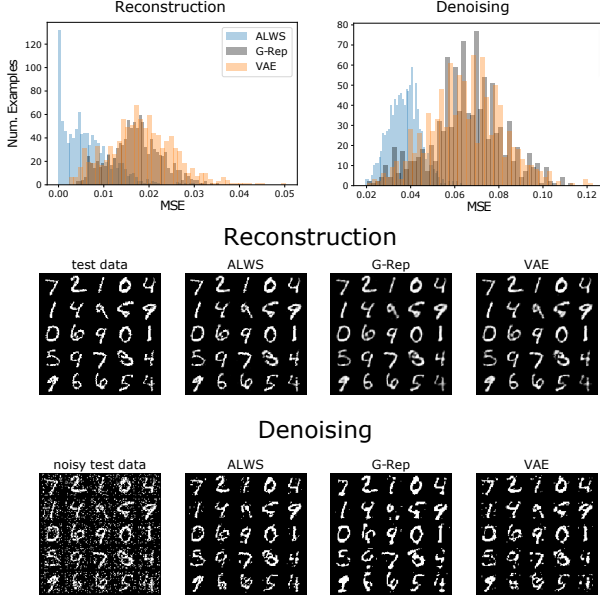


Figure 6. Beta-Gamma Matrix Factorisation. Top, mean squared error across 1,000 test inputs compared to G-Rep and VAE. Bottom, examples of real data, reconstructed and denoised samples.

Matrix Factorisation. A more accurate data model may improve performance on a downstream task that relies on inference of associated latent variables. Following (Ruiz et al., 2016), we test post-learning inference on a probabilistic non-negative matrix factorisation model:

$$p(z_i) = \mathcal{U}(z_i; 0, 1), \quad p(x_i|z) = \text{Bernoulli}(x_i; \bar{x}_i) \\ \bar{x}_i = \text{sigmoid}(\mathbf{w}_i \cdot \text{logit}(z) + b_i).$$

For each element of each \mathbf{w}_i , we place a penalty consistent with a $\text{Gamma}(w; 0.9, 0.3)$ prior on each entry and learn \mathbf{W} and \mathbf{b} . We include \mathbf{b} to the model trained by ALWS as it prevents samples with opposite colour polarity to be generated, which creates a more severe covariate shift that harms the gradient model. We evaluate the models on reconstructing and denoising handwritten digits from the binarised MNIST dataset. To recover the original image given a clean or noisy \mathbf{x}^* , we generate \mathbf{x} given the posterior mode found by maximising $\log p(\mathbf{z}, \mathbf{x}^*)$ over \mathbf{z} . We compare with a Bayesian version of the model trained by generalised reparameterisation Ruiz et al. (2016) and a VAE-like model in which the decoder has the generative structure as above and the posterior is a reparametrised Beta distribution. The results for both tasks are depicted in Figure 6. The leftmost panels show the histograms of MSE on 1 000 test images, and the other panels show examples of 25 test images and reconstructions by each method. ALWS achieved significantly lower error ($p < 10^{-10}$ for both a two-tailed t -test and a Wilcoxon signed-rank test).

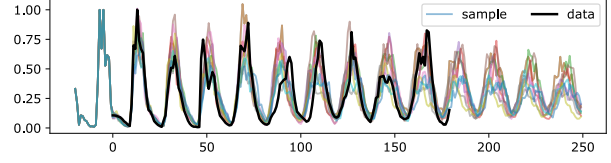


Figure 7. Modelling blowfly population time series. Black, training data. Coloured, samples for an extended time period drawn from the trained model.

4.5. Neural Processes

The neural process (NP) (Garnelo et al., 2018) is a model that learns to infer over functions. Conceptually, the computational goal of NPs is similar to predictive inference in Gaussian Processes, but without defining an explicit prior over functions. We review NPs in more detail and illustrate how they can be trained by ML using ALWS in Appendix C.5. We compared ALWS with the original variational learning method on a toy problem. NP trained by ALWS produces better prediction and uncertainty estimates on test inputs. See Figure 10 in Appendix C.5.

4.6. Dynamical Models

In fields such as biology and environmental science, the behaviour of complex systems is often described by simulation-based dynamical models. Estimating parameters for these models from data is crucial for prediction and policy-making. (Lintusaari et al., 2016; Sunnåker et al., 2013; Kypraios et al., 2017)

A dynamical model can be expressed, in discrete time, as

$$\mathbf{z}_t = \mathbf{l}_\theta(\mathbf{z}_{1:t-1}, \mathbf{x}_{1:t-1}, \mathbf{u}_t, \epsilon_t), \quad \mathbf{x}_t = \mathbf{o}_\theta(\mathbf{z}_t) + \mathbf{e}_t$$

where \mathbf{l}_θ describes a latent process that can depend on a control input \mathbf{u}_t , a noise source ϵ_t and the history of latents $\mathbf{z}_{1:t-1}$ and measurements $\mathbf{x}_{1:t-1}$. The function \mathbf{o}_θ maps the latent \mathbf{z}_t to measurement with noise \mathbf{e}_t . For ALWS, we need that $p_\theta(\mathbf{z}_t, \epsilon_t | \mathbf{z}_{1:t-1}, \mathbf{x}_{1:t-1}, \mathbf{u}_t)$ and $p_\theta(\mathbf{x}_t, \mathbf{e}_t | \mathbf{z}_t)$ are tractable so that $\nabla_\theta \log p(\mathbf{z}_{1:T}, \mathbf{x}_{1:T})$ can be evaluated, where T is the length of the data. However, learning using approximate inference may be challenging due to complex dependencies between latent variables and across time.

Here, we fit the parameters of two dynamical models: the Hodgkin-Huxley (HH) model (Pospischil et al., 2008) on the membrane potential of a simulated neuron, and an ecological model (ECO) on blowfly data (Wood, 2010). The HH equations describe the membrane potential and three ion-channel state variables of a neuron that follow complicated nonlinear transitions. Details of the experiment are in Appendix C.6. Results in Figure 12 show that the trained model can not only reproduce the training data well but also predict the response given new inputs \mathbf{u}_t . ECO describes nonlinear and non-Gaussian dynamics and has discrete and

continuous latent variables. Fitting ECO on blowfly data was used to validate approximate Bayesian computation (ABC) methods (Park et al., 2016). The model trained with ALWS can simulate sequences very close to data Figure 7, and are visibly closer than sequences from the model trained with ABC (Park et al., 2016, Figure 2b).

4.7. Sample Quality

Finally, we train deep models of images and test sample quality. We chose six benchmark datasets: the binarised and original MNIST (LeCun et al., 1998) (B-MNIST and MNIST, respectively), fashion MNIST (Fashion) (Xiao et al., 2017), natural images (Natural) (Hateren & Schaaf, 1998), CIFAR-10 (Krizhevsky et al., 2009) and CelebA (Liu et al., 2015). The original un-binarised MNIST is known to be difficult for most VAE-based methods (Loaiza-Ganem & Cunningham, 2019). Natural images consist of grey-scale images from natural scenes. All images have size 32×32 with colour channels. For ALWS, we test two variants. In ALWS-F, gradient model parameters γ are fixed. In ALWS-A, γ is adapted as described in Section 3.4 except for λ which is fixed at 0.1. Fixing λ improved quality for the higher-dimensional CIFAR-10 and CelebA, but lowered quality for Natural and did not affect much on the other datasets.

We compare these methods with four other approaches: the vanilla VAE (Kingma & Welling, 2014), VAE with a Sylvester (orthogonal) flow as an inference network (van den Berg et al., 2018) (Syl-VAE)⁵, semi-implicit variational inference (Yin & Zhou, 2018) (SIVI)⁶, and reweighted wake-sleep (Bornschein & Bengio, 2015). Each algorithm has the same generative network architecture as in DCGAN⁷ with the last convolutional layer removed. We also run WGAN-GP (Gulrajani et al., 2017)⁸ for reference, although it is not trained by ML methods. Each algorithm is run for 50 epochs ten times with different initialisations, except for SIVI where we trained for 1000 epochs with a lower learning rate for stability. To test the generative quality, we compute both the Fréchet Inception Distance (FID) (Heusel et al., 2017) and Kernel Inception Distance (KID) (Binkowski et al., 2018) on 10,000 generated images. The results are shown in Figure 8. According to FID, ALWS-A is the best ML method for binarised MNIST, Fashion, and CIFAR-10. Notably, both ALWS-A and ALWS-F have much smaller FID and KID on MNIST and Fashion than other ML methods. WGAN-GP did not produce a good score on CIFAR-10 within 50 epochs but becomes the best model for all datasets with further training. Samples are

shown from Figure 15 to Figure 20 in Appendix C.7 with additional experiments to show the effectiveness of ALWS.

5. Related Work

5.1. Amortised Variational Inference

Using $\mathcal{F}(q, \theta)$ as the objective for learning θ , the gradient for θ is given by an intractable posterior expectation. The large majority of learning algorithms based on amortised variational inference use Monte Carlo estimators for the gradient. The Variational auto-encoder (VAE) (Kingma & Welling, 2014; Rezende et al., 2014) parametrises $q_\phi(z|x)$ by simple distributions using reparameterised samples to obtain gradients for ψ . Approximate posteriors may also be incorporated into tighter bounds on $\log p_\theta(x)$ by reweighting (Burda et al., 2016; Bornschein & Bengio, 2015; Le et al., 2019), although with some loss of gradient signal (Rainforth et al., 2018). More expressive forms of q_ϕ can be formed by invertible transformations (normalising flows) (Rezende & Mohamed, 2015; Kingma et al., 2016; van den Berg et al., 2018) that allow $\mathbb{H}[q_\phi]$ to be computed easily, or by non-invertible mappings (implicit variational inference), which requires estimating $\mathbb{H}[q_\phi]$ or its gradient w.r.t. ϕ (Shi et al., 2018; Li & Turner, 2018; Yin & Zhou, 2018; Huszár, 2017). Reparametrising posterior samples may require non-trivial methods (Jang et al., 2017; Vahdat et al., 2018; Rolfe, 2017; Ruiz et al., 2016; Figurnov et al., 2018). On the other hand, amortised learning focuses exclusively on estimating the gradient for ML learning, making no assumptions on the type of latent variables.

Our approach is related to at least two other algorithms inspired by the original Helmholtz machine (HM) (Dayan et al., 1995; Hinton et al., 1995). The distributed distributional code HM (DDC-HM) (Vértes & Sahani, 2018) represents posteriors by expectations of pre-defined and finite nonlinear features, which are used to approximate $\Delta_{\theta_t}(x)$ by the linearity of expectation. ALWS differs from DDC-HM in two ways. First, our gradient model integrates the inferential model and the linear readout for $\Delta_{\theta_t}(x)$ in DDC-HM using adaptive and more flexible KRR. Second, using (9) avoids explicit computation of $\nabla_\theta \log p_\theta$ and makes ALWS easily applicable to more complex generative models. Reweighted wake-sleep (RWS) (Bornschein & Bengio, 2015) addressed covariance shift by training an inferential model to increase the likelihood of not only sleep z given sleep x as in the HM, but also weighted posterior samples given data x^* . ALWS does not make assumptions about the posterior distributions, and we found that simple strategies mitigated covariate shift in practice, but this is a point that deserves further investigation.

⁵github.com/rianevdborg/sylvester-flows

⁶github.com/mingzhang-yin/SIVI

⁷pytorch.org/tutorials/beginner/dcgan_faces_tutorial.html

⁸github.com/caogang/wgan-gp

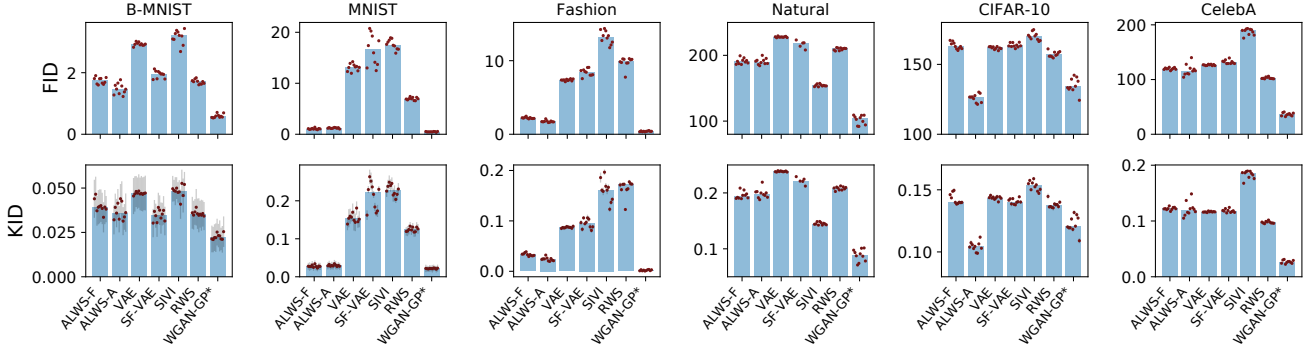


Figure 8. FID and KID scores (lower is better) for different datasets and methods. Red dot is the score for a single run. Bars are medians of the dots for each method. Short bars on KID dots shows standard error of the estimate. All models are trained for 50 epochs.

5.2. Training Implicit Generative Models

Implicit generative models, including generative adversarial networks (GANs) (Goodfellow et al., 2014) and simulation-based models considered by approximate Bayesian computation (ABC) (Tavaré et al., 1997; Marin et al., 2012), do not have an explicitly defined likelihood function but can be trained using simulated data. Amortised learning requires an explicit joint likelihood function $p_{\theta}(x, z)$, but can also train simulation-based generative models (Section 4.6). In GANs, the generator is improved by a discriminator that is concurrently trained to tell apart real and generated samples. The approach is able to synthesise high-quality samples in high dimensions. However, the competitive setting can be problematic for convergence, and the discriminator needs to be carefully regularised to be less effective at its own task but more informative to the generator. (Arjovsky et al., 2017; Gulrajani et al., 2017; Arbel et al., 2018; Mescheder et al., 2018). In amortised learning, a better gradient model always helps when training the generative model. Importantly, amortised learning can directly train real-world simulators for which samples of x are not differentiable w.r.t. θ , such as the Galton board, where GANs are not directly applicable.

Rather than performing maximum likelihood estimation, ABC estimates a posterior of θ using simulated data and a chosen prior on θ . Amortised learning can be seen as maximum likelihood learning based on simulations, since the gradient model is trained using data from the generative model. In particular, ALWS is similar to Kernel-ABC (Nakagome et al., 2013) in which the posterior is found by weighting prior samples using KRR on pre-defined summary statistics. The kernel recursive ABC (Kajihara et al., 2018) iteratively updates the prior over θ by herding from a kernel embedding (Song et al., 2009) of the posterior, converging to a maximum likelihood solution. ALWS does not maintain a distribution of θ , but iteratively updates them by gradient methods so that the model distribution approaches the data distribution. Also, ALWS performs well even when

the number of parameters is large for which traditional ABC methods are likely to be expensive.

6. Discussion

Direct estimation of the expected log-likelihood and its gradient in a latent variable model circumvents the challenges and issues posed by explicit approximation of posteriors. The KRR gradient model is consistent, easy to implement, and avoids the need for explicit computation of derivatives. However, we observe the following issues with the current instance of amortised learning. First, its computational complexity limits the number of sleep samples that can be used to train the gradient model and thus the quality of the approximation. Techniques such as random feature- and Nystrom-approximations could make KRR more efficient. Second, the KRR prediction is a linear combination of the set $\{\nabla_{\theta} \log p_{\theta}(z_n, x_n)\}_{n=1}^N$, but the true gradient function, which can be much higher-dimensional than N , may lie outside this span—an issue that might be compounded by covariate shift. Further, hyper-parameter learning using the meta-learning method described in Section 3.4 improves the estimation of J_{θ} rather than $\nabla_{\theta} J_{\theta}$, which might explain why adapting λ on some tasks worsens the results. Therefore, alternative amortised learning models may be worth future exploration. Nonetheless, we have found here that ALWS based on KRR provides accurate parameter estimates in many settings where approximate inference-based approaches appear to struggle.

ALWS can be extended to training generative models of other types of data, such as graphs, as long as an appropriate kernel is used. Another useful extension is to train conditional generative models, which we explored briefly in the neural processes experiment. In this case, the gradient model needs to depend on any conditioning variables (or sets). Finally, while we used LSR to approximate the gradient of the model w.r.t θ , other useful quantities could also be estimated in a similar fashion (Brehmer et al., 2020).

Acknowledgements

We thank Arthur Gretton, Sebastian Nowozin, Jiaxin Shi and Eszter Vértés for helpful discussions; we thank Ferenc Huszár for discussion and comments on an earlier draft.

References

- Arbel, M., Sutherland, D. J., Binkowski, M., and Gretton, A. On gradient regularizers for MMD GANs. In *NeurIPS*, pp. 6701–6711, 2018.
- Arjovsky, M., Chintala, S., and Bottou, L. Wasserstein generative adversarial networks. In *ICML*, 2017.
- Binkowski, M., Sutherland, D. J., Arbel, M., and Gretton, A. Demystifying MMD GANs. In *ICLR*, 2018.
- Bishop, C. M. *Pattern Recognition and Machine Learning*. Springer, 2006.
- Bornschein, J. and Bengio, Y. Reweighted wake-sleep. In *ICLR*, 2015.
- Boucheron, S., Lugosi, G., and Massart, P. *Concentration Inequalities: A Nonasymptotic Theory of Independence*. Oxford University Press, February 2013. ISBN 978-0-19-953525-5. doi: 10.1093/acprof:oso/9780199535255.001.0001.
- Bounliphone, W., Belilovsky, E., Blaschko, M. B., Antonoglou, I., and Gretton, A. A test of relative similarity for model selection in generative models. In *ICLR*, 2016.
- Brehmer, J., Louppe, G., Pavez, J., and Cranmer, K. Mining gold from implicit models to improve likelihood-free inference. *Proceedings of the National Academy of Sciences*, 117(10):5242–5249, 2020.
- Burda, Y., Grosse, R. B., and Salakhutdinov, R. Importance weighted autoencoders. In *ICLR*, 2016.
- Caponnetto, A. and De Vito, E. Optimal rates for the regularized least-squares algorithm. *Foundations of Computational Mathematics*, 2007.
- Carmeli, C., De Vito, E., and Toigo, A. Vector valued reproducing kernel Hilbert spaces of integrable functions and Mercer theorem. *Analysis and Applications*, 2006.
- Carmeli, C., De Vito, E., Toigo, A., and Umanitá, V. Vector valued reproducing kernel Hilbert spaces and universality. *Analysis and Applications*, 2010.
- Chatterjee, S., Diaconis, P., et al. The sample size required in importance sampling. *The Annals of Applied Probability*, 28(2):1099–1135, 2018.
- Davidson, T. R., Falorsi, L., Cao, N. D., Kipf, T., and Tomczak, J. M. Hyperspherical variational auto-encoders. In *UAI*, 2018.
- Dayan, P., Hinton, G. E., Neal, R. M., and Zemel, R. S. The Helmholtz machine. *Neural computation*, 1995.
- Dempster, A. P., Laird, N. M., and Rubin, D. B. Maximum likelihood from incomplete data via the em algorithm. *Journal of the Royal Statistical Society: Series B (Methodological)*, 1977.
- Dieng, A. B. and Paisley, J. Reweighted expectation maximization. *arXiv preprint arXiv:1906.05850*, 2019.
- Figurnov, M., Mohamed, S., and Mnih, A. Implicit reparameterization gradients. In *NeurIPS*, 2018.
- Garnelo, M., Schwarz, J., Rosenbaum, D., Viola, F., Rezende, D. J., Eslami, S., and Teh, Y. W. Neural processes. *arXiv preprint arXiv:1807.01622*, 2018.
- Goodfellow, I., Pouget-Abadie, J., Mirza, M., Xu, B., Warde-Farley, D., Ozair, S., Courville, A., and Bengio, Y. Generative adversarial nets. In *NeurIPS*, pp. 2672–2680, 2014.
- Gretton, A., Smola, A., Huang, J., Schmittfull, M., Borgwardt, K., and Schölkopf, B. Covariate shift by kernel mean matching. *Dataset shift in machine learning*, 2009.
- Gulrajani, I., Ahmed, F., Arjovsky, M., Dumoulin, V., and Courville, A. C. Improved training of Wasserstein GANs. In *NeurIPS*, 2017.
- Gutmann, M. and Hyvärinen, A. Noise-contrastive estimation: A new estimation principle for unnormalized statistical models. In *AISTATS*, 2010.
- Hateren, J. H. v. and Schaaf, A. v. d. Independent component filters of natural images compared with simple cells in primary visual cortex. *Proceedings: Biological Sciences*, 1998.
- Heusel, M., Ramsauer, H., Unterthiner, T., Nessler, B., and Hochreiter, S. GANs trained by a two time-scale update rule converge to a local Nash equilibrium. In *NeurIPS*, 2017.
- Hinton, G. E., Dayan, P., Frey, B. J., and Neal, R. M. The “wake-sleep” algorithm for unsupervised neural networks. *Science*, 1995.
- Hofmann, T., Schölkopf, B., and Smola, A. J. Kernel methods in machine learning. *The annals of statistics*, 2008.
- Huggins, J. H., Kasprzak, M., Campbell, T., and Broderick, T. Practical posterior error bounds from variational objectives. *CoRR*, abs/1910.04102, 2019.

- Huszár, F. Variational inference using implicit distributions. *arXiv preprint arXiv:1702.08235*, 2017.
- Hyvärinen, A. and Oja, E. Independent component analysis: algorithms and applications. *Neural Networks*, 2000.
- Jang, E., Gu, S., and Poole, B. Categorical reparameterization with gumbel-softmax. In *ICLR*, 2017.
- Johnson, M., Duvenaud, D. K., Wiltchko, A., Adams, R. P., and Datta, S. R. Composing graphical models with neural networks for structured representations and fast inference. In *NeurIPS*, pp. 2946–2954, 2016.
- Kajihara, T., Kanagawa, M., Yamazaki, K., and Fukumizu, K. Kernel recursive abc: Point estimation with intractable likelihood. In *International Conference on Machine Learning*, pp. 2400–2409, 2018.
- Kingma, D. P. and Welling, M. Auto-encoding variational Bayes. In *2nd International Conference on Learning Representations, ICLR 2014, Banff, AB, Canada, April 14-16, 2014, Conference Track Proceedings*, 2014.
- Kingma, D. P., Salimans, T., Jozefowicz, R., Chen, X., Sutskever, I., and Welling, M. Improved variational inference with inverse autoregressive flow. In *NIPS*, pp. 4743–4751, 2016.
- Krizhevsky, A., Hinton, G., et al. Learning multiple layers of features from tiny images. Technical report, 2009.
- Kypriaios, T., Neal, P., and Prangle, D. A tutorial introduction to Bayesian inference for stochastic epidemic models using Approximate Bayesian Computation. *Mathematical biosciences*, 2017.
- Le, T. A., Kosiorek, A. R., Siddharth, N., Teh, Y. W., and Wood, F. Revisiting reweighted wake-sleep for models with stochastic control flow. In *UAI*, 2019.
- LeCun, Y., Bottou, L., Bengio, Y., Haffner, P., et al. Gradient-based learning applied to document recognition. *Proceedings of the IEEE*, 86(11):2278–2324, 1998.
- Li, Y. and Turner, R. E. Gradient estimators for implicit models. In *ICLR*, 2018.
- Lin, W., Hubacher, N., and Khan, M. E. Variational message passing with structured inference networks. In *ICLR*, 2018.
- Lintusaari, J., Gutmann, M. U., Dutta, R., Kaski, S., and Corander, J. Fundamentals and Recent Developments in Approximate Bayesian Computation. *Systematic Biology*, 2016.
- Liu, Z., Luo, P., Wang, X., and Tang, X. Deep learning face attributes in the wild. In *ICCV*, 2015.
- Loaiza-Ganem, G. and Cunningham, J. P. The continuous Bernoulli: fixing a pervasive error in variational autoencoders. In *NeurIPS*, 2019.
- Marin, J.-M., Pudlo, P., Robert, C. P., and Ryder, R. J. Approximate Bayesian computational methods. *Statistics and Computing*, 2012.
- Mathieu, E., Le Lan, C., Maddison, C. J., Tomioka, R., and Teh, Y. W. Continuous hierarchical representations with Poincaré variational auto-encoders. In *NeurIPS*, 2019.
- Mescheder, L. M., Geiger, A., and Nowozin, S. Which training methods for GANs do actually converge? In *ICML*, 2018.
- Nagano, Y., Yamaguchi, S., Fujita, Y., and Koyama, M. A wrapped normal distribution on hyperbolic space for gradient-based learning. In *ICML*, 2019.
- Nakagome, S., Fukumizu, K., and Mano, S. Kernel approximate bayesian computation in population genetic inferences. *Statistical applications in genetics and molecular biology*, 2013.
- Newey, K. and McFadden, D. Large sample estimation and hypothesis. *Handbook of Econometrics, IV, Edited by RF Engle and DL McFadden*, 1994.
- Park, M., Jitkrittum, W., and Sejdinovic, D. K2-ABC: Approximate Bayesian Computation with kernel embeddings. In *AISTATS*, 2016.
- Pospischil, M., Toledo-Rodriguez, M., Monier, C., Piwkowska, Z., Bal, T., Frégnac, Y., Markram, H., and Destexhe, A. Minimal Hodgkin–Huxley type models for different classes of cortical and thalamic neurons. *Biological cybernetics*, 2008.
- Rainforth, T., Kosiorek, A. R., Le, T. A., Maddison, C. J., Igl, M., Wood, F., and Teh, Y. W. Tighter variational bounds are not necessarily better. In *ICML*, 2018.
- Rezende, D. and Mohamed, S. Variational inference with normalizing flows. In *ICML*, 2015.
- Rezende, D. J., Mohamed, S., and Wierstra, D. Stochastic backpropagation and approximate inference in deep generative models. In *ICML*, pp. 1278–1286, 2014.
- Rolfe, J. T. Discrete variational autoencoders. In *ICLR*, 2017.
- Ruiz, F. J. R., Titsias, M. K., and Blei, D. M. The generalized reparameterization gradient. In *NeurIPS*, 2016.
- Shi, J., Sun, S., and Zhu, J. Kernel implicit variational inference. In *ICLR*, 2018.

- Shimodaira, H. Improving predictive inference under covariate shift by weighting the log-likelihood function. *Journal of statistical planning and inference*, 2000.
- Song, L., Huang, J., Smola, A., and Fukumizu, K. Hilbert space embeddings of conditional distributions with applications to dynamical systems. In *ICML*, 2009.
- Sunnåker, M., Busetto, A. G., Numminen, E., Corander, J., Foll, M., and Dessimoz, C. Approximate Bayesian Computation. *PLoS CB*, 2013.
- Szabó, Z., Sriperumbudur, B. K., Póczos, B., and Gretton, A. Learning theory for distribution regression. *Journal of Machine Learning Research*, 2016.
- Tavaré, S., Balding, D. J., Griffiths, R. C., and Donnelly, P. Inferring coalescence times from DNA sequence data. *Genetics*, 1997.
- Turner, R. and Sahani, M. Two problems with variational expectation maximisation for time-series models. *Bayesian Time Series Models*, 2011.
- Vahdat, A., Macready, W. G., Bian, Z., Khoshaman, A., and Andriyash, E. DVAE++: Discrete variational autoencoders with overlapping transformations. In *ICML*, 2018.
- van den Berg, R., Hasenclever, L., Tomczak, J. M., and Welling, M. Sylvester normalizing flows for variational inference. In *Proceedings of the Thirty-Fourth Conference on Uncertainty in Artificial Intelligence, UAI 2018, Monterey, California, USA, August 6-10, 2018*, pp. 393–402, 2018.
- Vértes, E. and Sahani, M. Flexible and accurate inference and learning for deep generative models. In *NeurIPS*, pp. 4166–4175, 2018.
- Wenliang, L., Sutherland, D. J., Strathmann, H., and Gretton, A. Learning deep kernels for exponential family densities. In *ICML*, 2019.
- Wenliang, L. K. and Sahani, M. A neurally plausible model for online recognition and postdiction in a dynamical environment. In *NeurIPS*, 2019.
- Wilson, A. G., Hu, Z., Salakhutdinov, R., and Xing, E. P. Deep kernel learning. In *AISTATS*, 2016.
- Wood, S. N. Statistical inference for noisy nonlinear ecological dynamic systems. *Nature*, 2010.
- Xiao, H., Rasul, K., and Vollgraf, R. Fashion-MNIST: a novel image dataset for benchmarking machine learning algorithms. *arXiv preprint arXiv:1708.07747*, 2017.
- Xu, J. and Durrett, G. Spherical latent spaces for stable variational autoencoders. *EMNLP*, 2018.
- Yin, M. and Zhou, M. Semi-implicit variational inference. In *ICML*, 2018.
- Zhang, C., Butepage, J., Kjellstrom, H., and Mandt, S. Advances in variational inference. *Pattern analysis and machine intelligence*, 2018.

A. Mathematical details

A.1. Solving mean squared error for conditional expectations

Given $\mathbf{x}, \mathbf{y} \sim \rho(\mathbf{x}, \mathbf{y})$, we want to find an estimator in some space \mathcal{F} of the posterior mean function $\mathbf{f}_\rho : \mathbf{x} \mapsto \mathbb{E}_{\rho(\mathbf{y}|\mathbf{x})}[\mathbf{y}]$. Assuming that \mathcal{F} is contained in \mathcal{L}_ρ^2 , the class of squared-integral functions under $\rho(\mathbf{x})$, and that \mathbf{y} has finite l -2 norm under $\rho(\mathbf{y})$, a natural cost function to learn \mathbf{f} is the expected squared l -2 distance

$$L_E(\mathbf{f}) := \mathbb{E}_{\rho(\mathbf{y}, \mathbf{x})} [\|\mathbf{f}(\mathbf{x}) - \mathbf{y}\|_2^2] = \mathbb{E}_{\rho(\mathbf{x})} [\mathbb{E}_{\rho(\mathbf{y}|\mathbf{x})} [\|\mathbf{f}(\mathbf{x}) - \mathbf{y}\|_2^2]].$$

By Jensen's inequality,

$$L_E(\mathbf{f}) \leq \mathbb{E}_{\rho(\mathbf{x})} [\|\mathbf{f}(\mathbf{x}) - \mathbb{E}_{\rho(\mathbf{y}|\mathbf{x})}[\mathbf{y}]\|_2^2] = L_R(\mathbf{f}).$$

This shows that the MSE is an upper bound on the expected l -2 distance between $\mathbf{f}(\mathbf{x})$ and the posterior mean $\mathbb{E}_{\rho(\mathbf{y}|\mathbf{x})}[\mathbf{y}]$. Further, the minimum of L_R is attained at an \mathbf{f} that also minimises L_E . This can be shown through a simple decomposition

$$\begin{aligned} L_E(\mathbf{f}) &= \mathbb{E}_{\rho(\mathbf{x})} [\mathbb{E}_{\rho(\mathbf{y}|\mathbf{x})} [\|\mathbf{f}(\mathbf{x}) - \mathbf{y}\|_2^2]] \\ &= \mathbb{E}_{\rho(\mathbf{x})} [\|\mathbf{f}(\mathbf{x})\|_2^2 - \mathbf{f}(\mathbf{x}) \cdot \mathbb{E}_{\rho(\mathbf{y}|\mathbf{x})}[\mathbf{y}] + \mathbb{E}_{\rho(\mathbf{y}|\mathbf{x})} [\|\mathbf{y}\|_2^2]] \\ &\stackrel{(1)}{=} \mathbb{E}_{\rho(\mathbf{x})} [\|\mathbf{f}(\mathbf{x})\|_2^2 - \mathbf{f}(\mathbf{x}) \cdot \mathbb{E}_{\rho(\mathbf{y}|\mathbf{x})}[\mathbf{y}] + \|\mathbb{E}_{\rho(\mathbf{y}|\mathbf{x})}[\mathbf{y}]\|_2^2 + \text{Tr} [\mathbb{C}_{\rho(\mathbf{y}|\mathbf{x})}[\mathbf{y}]]] \\ &= \mathbb{E}_{\rho(\mathbf{x})} [\mathbb{E}_{\rho(\mathbf{y}|\mathbf{x})} [\|\mathbf{f}(\mathbf{x}) - \mathbb{E}_{\rho(\mathbf{y}|\mathbf{x})}[\mathbf{y}]\|_2^2]] + \mathbb{E}_{\rho(\mathbf{x})} [\text{Tr} [\mathbb{C}_{\rho(\mathbf{y}|\mathbf{x})}(\mathbf{y})]] \\ &= L_R(\mathbf{f}) + \text{term independent of } \mathbf{f} \end{aligned}$$

where \mathbb{C}_p is the covariance under p . Equality (1) holds because

$$\mathbb{E}_p [\|\mathbf{a}\|_2^2] = \mathbb{E}_p \left[\sum_i a_i^2 \right] = \sum_i \mathbb{E}_p [a_i^2] = \mathbb{E}_p [a_i]^2 + \sum_i \mathbb{V}_p [a_i] = \|\mathbb{E}_p [\mathbf{a}]\|_2^2 + \text{Tr} [\mathbb{C}_p [\mathbf{a}]]$$

for any $\mathbf{a} \in \mathcal{L}_p^2$. So $L_R(\mathbf{f})$ is equal to $L_E(\mathbf{f})$ up to a constant that depends only on ρ but not \mathbf{f} .

A.2. Boundedness of the gradient function

To learn $\mathbf{y}(\mathbf{x}) = \mathbb{E}_{p_{\theta_t}(\mathbf{z}|\mathbf{x})} [\nabla_{\theta} \log p_{\theta}(\mathbf{z}, \mathbf{x})]_{\theta_t}$ using regression as above, the target needs to be square-integrable under $p_{\theta_t}(\mathbf{x})$, i.e. $\mathbf{y}(\mathbf{x}) \in \mathcal{L}_p^2$. Common likelihood functions are in the exponential family and has $\nabla_{\theta} \log p_{\theta}(\mathbf{z}, \mathbf{x}) = \nabla_{\theta} \boldsymbol{\eta}(\mathbf{z}) \mathbf{s}(\mathbf{x}) - \nabla_{\theta} \Psi(\mathbf{z})$. Thus, it suffices to check the \mathcal{L}_p^2 integrability of the gradient in terms of these functions. We sketch below that this is indeed the case for common choices of model architectures.

As a simple example, consider a model

$$p_{\theta}(\mathbf{z}) = \mathcal{N}(\mathbf{0}, \mathbf{I}), \quad p_{\theta}(\mathbf{x}|\mathbf{z}) = \mathcal{N}(\text{NN}_{\mathbf{w}}(\mathbf{z}), \boldsymbol{\Sigma}). \quad (14)$$

where \mathbf{I} is the identity covariance matrix, $\text{NN}_{\mathbf{w}}$ is a neural network with weights \mathbf{w} and $\boldsymbol{\Sigma}$ is a diagonal matrix. Note that in this case, one has that

$$\Psi_{\theta}(\mathbf{z}) = -\frac{1}{2} \|\mathbf{z}\|_2^2 - \frac{1}{2} \log |\boldsymbol{\Sigma}| + \text{constant}, \quad \boldsymbol{\eta}_{\theta}(\mathbf{z}) = [\boldsymbol{\Sigma}^{-1} \text{NN}_{\mathbf{w}}(\mathbf{z}), -\frac{1}{2} \boldsymbol{\Sigma}^{-1}], \quad \theta = \{\mathbf{w}, \boldsymbol{\Sigma}\}, \quad \mathbf{s}(\mathbf{x}) = [\mathbf{x}, \mathbf{x}\mathbf{x}^T].$$

Further, assume that

1. The neural network $\text{NN}_{\mathbf{w}}(\mathbf{z})$ is Lipschitz and \mathbf{w} -differentiable almost everywhere, such as one that is composed of linear projections followed by Lipschitz nonlinearities (e.g., ReLU).
2. $\mathbb{E}_{p_{\theta}(\mathbf{z})} [\|\text{NN}_{\mathbf{w}}(\mathbf{z})\|_2^2] < \infty$.
3. Spectral norm of weights \mathbf{W} in each layer of $\text{NN}_{\mathbf{w}}(\mathbf{z})$ is bounded above by a positive constant.

4. The diagonal elements of Σ are bounded below by some constant.

The first and second assumptions are mild and satisfied by NNs with ReLU activations. The third and fourth conditions limit the ranges of the parameter values, which can be imposed by clipping or through appropriate parametrisation.

The second and fourth conditions make the gradients of $\Psi_\theta(z)$ and $\eta_\theta(z)$ w.r.t. Σ bounded; thus, we will demonstrate the integrability of the gradients w.r.t. the neural network parameter w .

First term $\mathbb{E}_{p_\theta(z|x)}[\nabla_\theta \eta_\theta(z)]s(x)$

Multiple applications of the Cauchy-Schwartz inequality yields

$$\mathbb{E}_{p_\theta(x)} \left[\left\| \mathbb{E}_{p_\theta(z|x)} [\nabla_w \eta_\theta(z)] s(x) \right\|^2 \right] \leq \sqrt{\mathbb{E}_{p_\theta(x)} \left[\left\| \mathbb{E}_{p_\theta(z|x)} [\nabla_w \eta_\theta(z)] \right\|_2^4 \right]} \sqrt{\mathbb{E}_{p_\theta(x)} \left[\|s(x)\|_2^4 \right]}.$$

By our assumption, $\text{NN}(z)$ is Lipschitz w.r.t. w and the gradient $\nabla_w \eta_\theta(z)$ is bounded as, for $C_0, C_1 > 0$, $\|\nabla_w \eta_\theta(z)\|_2 \leq C_0 + C_1 \|z\|_2$. This can be proved by writing out $\nabla_w \text{NN}_\theta(z)$ using the chain rule, which will be a series of product involving W in each layer and derivative of Lipschitz functions, and applying the first two conditions above. Thus, we have

$$\begin{aligned} \mathbb{E}_{p_\theta(x)} \left[\left\| \mathbb{E}_{p_\theta(z|x)} [\nabla_w \eta_\theta(z)] \right\|_2^4 \right] &\leq \mathbb{E}_{p_\theta(x)} \left[\mathbb{E}_{p_\theta(z|x)} \left[\|\nabla_w \eta_\theta(z)\|_2^4 \right] \right] \\ &\leq \mathbb{E}_{p_\theta(z)} \left[(C_0 + C_1 \|z\|_2)^4 \right] < \infty \end{aligned}$$

as the prior $p_\theta(z)$ is a standard Gaussian.

The integrability of $s(x)$ is equivalent to the finiteness of the corresponding moments of $p_\theta(x)$. By Lemma A.2, the marginal $p_\theta(x)$ has exponential tails, and thus the moments are finite.

Second term $\nabla_\theta \Psi(z)$

$$\mathbb{E}_{p_{\theta_t}(z)} \left[\left\| \mathbb{E}_{p_{\theta_t}(z|x)} [\nabla_\theta \Psi_\theta(z)] \right\|_2^2 \right] \leq \mathbb{E}_{p_{\theta_t}(z)} \left[\mathbb{E}_{p_{\theta_t}(z|x)} \left[\|\nabla_\theta \Psi_\theta(z)\|_2^2 \right] \right] = \|\Sigma^{-1}\|_2^2 < \infty$$

where we have applied Jensen's inequality. Therefore, $\mathbb{E}_{p_\theta(z|x)}[\nabla_\theta \Psi(z)]$ is a finite constant and thus in \mathcal{L}_p^2 .

Therefore, for the generative model defined in (14), the desired target $y(x) = \mathbb{E}_{p_{\theta_t}(z|x)}[\nabla_\theta \log p_\theta(z, x)]|_{\theta_t}$ for regression is in \mathcal{L}_p^2 , which can be approximated arbitrarily well by KRR (see Section 2.4)) with more sleep samples. A similar analysis can show that for Bernoulli likelihoods whose logits are parametrised by a Lipschitz neural network, the target for the regression is also in \mathcal{L}_p^2 , with logits bounded from above and below.

A.3. Gradient of the log marginal likelihood w.r.t. parameters

To show the result used in (7), we start from the free energy (ELBO) lower bound on the log-likelihood $\log p_\theta(x)$.

$$\begin{aligned} \log p_\theta(x) &= \log \frac{p_\theta(z, x)}{p_\theta(z|x)} = \int q(z) \log \left[\frac{q(z)}{q(z)} \frac{p_\theta(z, x)}{p_\theta(z|x)} \right] dz = \int q(z) \log \left[\frac{p_\theta(z, x)}{q(z)} \frac{q(z)}{p_\theta(z|x)} \right] dz \\ &= \int q(z) \log p_\theta(z, x) dz - \int q(z) \log q(z) dz + D_{\text{KL}}[q(z) \| p_\theta(z|x)] \\ &= \mathcal{F}(q, \theta) + D_{\text{KL}}[q(z) \| p_\theta(z|x)], \end{aligned} \tag{15}$$

where we have defined

$$\mathcal{F}(q, \theta) = \int q(z) \log p_\theta(z, x) dz - \int q(z) \log q(z) dz = \mathbb{E}_{q(z)}[\log p_\theta(z, x)] + \mathbb{H}[q].$$

The KL term in (15) is non-negative and is zero if $q(z) = p_\theta(z|x)$, suggesting that

$$\log p_\theta(x) = \mathcal{F}(p_\theta(z|x), \theta)$$

Replacing $q(z) = p_\theta(z|x)$ in (15) and take derivative w.r.t. θ gives (assuming all derivatives and expectations exist)

$$\begin{aligned}\Delta_\theta(x) &:= \nabla_\theta \log p_\theta(x) \\ &= \nabla_\theta \int p_\theta(z|x) \log p_\theta(z, x) dz - \nabla_\theta \int p_\theta(z|x) \log p_\theta(z|x) dz \\ &= \int \nabla_\theta p_\theta(z|x) \log p_\theta(z, x) dz + \int p_\theta(z|x) \nabla_\theta \log p_\theta(z, x) dz \\ &\quad - \int \nabla_\theta p_\theta(z|x) \log p_\theta(z|x) dz - \int p_\theta(z|x) \nabla_\theta \log p_\theta(z|x) dz.\end{aligned}\tag{16}$$

The last term in (16) is zero since it is the expectation of the score function

$$\int p_\theta(z|x) \nabla \log p_\theta(z|x) dz = \int p_\theta(z|x) \frac{1}{p_\theta(z|x)} \nabla_\theta p_\theta(z|x) dz = \nabla_\theta \int p_\theta(z|x) dz = 0.$$

The first and third terms in (16) combines to give

$$\int \nabla_\theta p_\theta(z|x) \log \frac{p_\theta(z, x)}{p_\theta(z|x)} dz = \int \nabla_\theta p_\theta(z|x) \log p_\theta(x) dz = \log p_\theta(x) \nabla_\theta \int p_\theta(z|x) dz = 0.$$

We are left with only the second term in (16)

$$\Delta_\theta(x) = \int p_\theta(z|x) \nabla_\theta \log p_\theta(z, x) = \mathbb{E}_{p_\theta(z|x)} [\nabla_\theta \log p_\theta(z, x)] = \nabla_\theta \mathcal{F}(p_\theta(z|x), \theta).\tag{17}$$

To compute the update at the t 'th iteration with $\theta = \theta_t$, and the expectation above is taken over a fixed posterior distribution $p_{\theta_t}(z|x)$. We evaluate the above equation at θ_t , giving (7),

$$\Delta_{\theta_t}(x) := \Delta_\theta(x)|_{\theta_t} = \nabla_\theta \mathbb{E}_{p_{\theta_t}(z|x)} [\log p_\theta(z, x)]|_{\theta_t} = \nabla_\theta \mathcal{F}(p_\theta(z|x), \theta)|_{\theta_t}.$$

One can also pass ∇_θ and its evaluation inside the expectation (assuming derivatives exist) to obtain (8)

$$\Delta_{\theta_t}(x) = \nabla_\theta \mathbb{E}_{p_{\theta_t}(z|x)} [\log p_\theta(z, x)]|_{\theta_t} = \mathbb{E}_{p_{\theta_t}(z|x)} [\nabla_\theta \log p_\theta(z, x)]|_{\theta_t}$$

which is used for direct gradient estimation.

In fact, once we know the result above, going from the right-hand side to the left is much simpler:

$$\begin{aligned}\mathbb{E}_{p_{\theta_t}(z|x)} [\nabla_\theta \log p_\theta(z, x)]|_{\theta_t} &= \mathbb{E}_{p_{\theta_t}(z|x)} [\nabla_\theta \log p_\theta(z|x)|_{\theta_t} + \nabla_\theta \log p_\theta(x)|_{\theta_t}] \\ &= \nabla_\theta \mathbb{E}_{p_{\theta_t}(z|x)} [\log p_\theta(z|x)]|_{\theta_t} + \nabla_\theta \log p_\theta(x)|_{\theta_t} \\ &= 0 + \Delta_{\theta_t}(x).\end{aligned}$$

Additionally, a quicker and more direct way to obtain (17) uses the ‘‘score trick’’ as follows

$$\nabla \log p_\theta(x) = \frac{1}{p_\theta(x)} \nabla_\theta \int p_\theta(z, x) dz = \frac{1}{p_\theta(x)} \int p_\theta(z, x) \nabla_\theta \log p_\theta(z, x) dz = \mathbb{E}_{p_\theta(z|x)} [\nabla_\theta \log p_\theta(z, x)].$$

A.4. Miscellaneous results

Theorem A.1 (Gaussian concentration inequality (Boucheron et al., 2013, Theorem 5.6)). *Let $X = (X_1, \dots, X_n)$ be a vector of n independent standard normal random variables. Let $f : \mathbb{R}^n \rightarrow \mathbb{R}$ denote an L -Lipschitz function. Then, all $t > 0$,*

$$P[f(X) - \mathbb{E}f(X) \geq t] \leq e^{-t^2/(2L^2)}.$$

Lemma A.2. *Let s^2 be the sum of the diagonal elements of Σ . Assume $\mathbb{E}_Z[\|\text{NN}_w(Z)\|_2] < \infty$. For the density function $p_\theta(x)$ defined in (14), for all $t > 2s$, we have*

$$P(\|X\| - \mathbb{E}\|X\| \geq t) \leq 2(e^{-\frac{t^2}{8L_1^2}} + e^{-\frac{(t/2-s)^2}{2L_2^2}})$$

Proof. Note that

$$P(\|X\| - \mathbb{E}\|X\| \geq t) \leq P(\|X\| - \mathbb{E}\|X\| \geq t) + P(-\|X\| + \mathbb{E}\|X\| \geq t).$$

We bound the first term below (the second term can be handled similarly).

We have

$$\begin{aligned} P(\|X\|_2 - \mathbb{E}\|X\|_2 \geq t) &= \mathbb{E}_Z[P(\|X\|_2 - \mathbb{E}\|X\|_2 \geq t|Z)] \\ &\leq \mathbb{E}_Z[P(\|X\|_2 - \mathbb{E}_{X|Z}[\|X\|_2] \geq t/2|Z)] + P(\mathbb{E}_{X|Z}[\|X\|_2] - \mathbb{E}\|X\|_2 \geq t/2). \end{aligned}$$

By Theorem A.1, as $p_\theta(\mathbf{x}|z) = \mathcal{N}(\text{NN}_w(z), \Sigma)$,

$$P(\|X\|_2 - \mathbb{E}_{X|Z}[\|X\|_2] \geq t/2|Z) \leq e^{-\frac{t^2}{8L_1^2}},$$

where $L_1 = \|\Sigma^{1/2}\|_{\text{op}}$ is the operator norm of $\Sigma^{1/2}$. Therefore,

$$\mathbb{E}_Z[P(\|X\|_2 - \mathbb{E}_{X|Z}[\|X\|_2] \geq t/2|Z)] \leq e^{-\frac{t^2}{8L_1^2}}.$$

Let $\mu(z) = \text{NN}_w(z)$. For the second term, as

$$\begin{aligned} \mathbb{E}_{X|Z}[\|X\|_2] &\leq \sqrt{\mathbb{E}_{X|Z}[\|X - \mu(Z)\|_2^2]} + \|\mu(Z)\|_2 = s + \|\mu(Z)\|_2, \\ \mathbb{E}_Z[\|\mu(Z)\|_2] &= \mathbb{E}_Z[\|\mathbb{E}_{X|Z}[X]\|_2] \leq \mathbb{E}_Z[\mathbb{E}_{X|Z}[\|X\|_2]] = \mathbb{E}_X[\|X\|_2], \end{aligned}$$

we have

$$P(\mathbb{E}_{X|Z}[\|X\|_2] - \mathbb{E}\|X\|_2 \geq t/2) \leq P(\|\mu(Z)\| - \mathbb{E}_Z[\|\mu(Z)\|] \geq t/2 - s).$$

By the Lipschitzness of $\text{NN}_w(z)$ and $p_\theta(z) = \mathcal{N}(0, \mathbf{I})$, we have for all $t > 2s$

$$P(\|\mu(Z)\| - \mathbb{E}_Z[\|\mu(Z)\|] \geq t/2 - s) \leq e^{-\frac{(t/2-s)^2}{2L_2^2}},$$

where L_2 is the Lipschitz constant of NN_w (as a function of z). Combining these bounds gives

$$P(\|X\|_2 - \mathbb{E}\|X\|_2 \geq t) \leq e^{-\frac{t^2}{8L_1^2}} + e^{-\frac{(t/2-s)^2}{2L_2^2}}$$

□

B. Method details

B.1. Alternative gradient models

To ensure that the estimate of J_θ can be differentiated w.r.t. θ to obtain an estimate of $\Delta_{\theta_t}(\mathbf{x})$, the gradient model needs to depend on model parameter θ . KRR satisfies this condition in an attractive way, because its prediction depends on θ and γ in two separate factors, see (12). However, though theoretically consistent, KRR estimates the gradient at the cost of N^3 in memory and time, where N is the number of sleep samples. We discuss two alternative gradient models that could potentially be much faster, but there is no theoretical guarantee that $\nabla_{\theta} \hat{J}_{\theta, \gamma}|_{\theta_t}$ is close to $\Delta_{\theta_t}(\mathbf{x})$.

B.1.1. GENERIC FUNCTION APPROXIMATOR

One can train a generic function estimator, such as a neural network, to estimate $J_\theta(\mathbf{x})$. For such parametric models, the dependence on generative model parameters θ can be encapsulated into gradient model parameters γ through gradient descent.

$$\gamma(\theta) \leftarrow \gamma(\theta) - \alpha \nabla_{\gamma} L(\theta, \gamma), \quad L(\theta, \gamma) = \sum_{n=1}^N |\hat{J}_{\gamma(\theta)}(\mathbf{x}_n) - \log p_{\theta}(\mathbf{z}_n, \mathbf{x}_n)|^2$$

where α is the learning rate. As such, the estimator of J_θ is better denoted as $\hat{J}_{\gamma(\theta)}$ for a neural network with fixed hyperparameters. Evaluating $\nabla_\theta \hat{J}_{\gamma(\theta)}|_{\theta_t}$ can be implemented, though less straightforwardly compared to the KRR gradient model. Alternatively, we can consider small perturbations around fixed-point of the loss, and derive a relationship between γ and θ at a local minimum:

$$0 = \frac{\partial L}{\partial \gamma}(\theta + d\theta, \gamma(\theta + d\theta)) = \frac{\partial L}{\partial \gamma}(\theta, \gamma(\theta)) + d\theta \frac{\partial}{\partial \theta} \frac{\partial L}{\partial \gamma}(\theta, \gamma(\theta)) + d\gamma \frac{\partial}{\partial \gamma} \frac{\partial L}{\partial \gamma}(\theta, \gamma(\theta)).$$

The first term on the RHS is zero, and rearranging gives $\frac{d\gamma(\theta)}{d\theta} = - \left(\frac{\partial^2 L}{\partial \gamma \partial \gamma} \right)^{-1} \frac{\partial^2 L}{\partial \theta \partial \gamma}$, assuming the inverse exists. Thus,

$$\frac{d\hat{J}_{\gamma(\theta)}(x)}{d\theta} = \frac{\partial \hat{J}_{\gamma(\theta)}(x)}{\partial \gamma} \frac{d\gamma(\theta)}{d\theta} = - \frac{\partial \hat{J}_{\gamma(\theta)}(x)}{\partial \gamma} \left(\frac{\partial^2 L}{\partial \gamma \partial \gamma} \right)^{-1} \frac{\partial^2 L}{\partial \theta \partial \gamma}.$$

All of the factors can be computed by automatic differentiation since the objects being differentiated are all scalars. However, for a generic neural network, the Hessian of the loss w.r.t. γ may not exist, and computing it can be unstable.

B.1.2. PARTICLE ESTIMATOR

The prediction of the KRR estimator may not but a valid expectation. In other words, $\hat{J}_{\theta, \gamma}(x)$ may not correspond to the expected log joint under any valid probability distribution. To address this issue, we can approximate $\Delta_{\theta_t}(x)$ through a set of particles z' (in the space of the latent) generated from a simulator $S_\gamma : (x, n) \rightarrow z'$, where γ is the parameter of the simulator, x is an observation, and n is a noise source distributed as $\zeta(n)$. For all x from the generative model, we want the simulator to produce particles such that $\mathbb{E}_{\zeta(n)}[\nabla_\theta \log p_\theta(S_\gamma(x, n), x)]|_{\theta_t}$ estimates of $\Delta_{\theta_t}(x)$. This can be achieved by solving

$$\min_{\gamma} \mathbb{E}_{p_{\theta_t}(z, x)} \left[\left\| \mathbb{E}_{p(n)}[\nabla_\theta \log p_\theta(S_\gamma(x, n), x)]|_{\theta_t} - \nabla_\theta \log p_\theta(z, x)|_{\theta_t} \right\|^2 \right],$$

which is equivalent to

$$\min_{\gamma} \mathbb{E}_{p_{\theta_t}(x)} \left[\left\| \mathbb{E}_{p(n)}[\nabla_\theta \log p_\theta(S_\gamma(x, n), x)]|_{\theta_t} - \mathbb{E}_{p_{\theta_t}(z|x)}[\nabla_\theta \log p_\theta(z, x)|_{\theta_t}] \right\|^2 \right]$$

due to the property of mean squared error (see Appendix A.1). We know that the optimal set of particles is distributed as the posterior $p_{\theta_t}(z|x)$, but minimising the cost above does not necessarily drive S_γ to produce posterior samples. Nonetheless, this set of particles is adequate to approximate $\Delta_{\theta_t}(x)$. We refer to this scheme as amortised learning by particles (AL-P). We test this on sample quality experiments and found that the KIDs and FIDs were in general worse than even the vanilla VAE. Samples from the model trained by AL-P are shown in Figure 15 to Figure 20 in section Appendix C.7.

B.1.3. RELATIONSHIP BETWEEN KRR GRADIENT MODEL AND IMPORTANCE SAMPLING

The KRR gradient model approximates $\Delta_{\theta_t}(x)$ by linearly weighting $\{\nabla_\theta \log p_\theta(z_n, x_n)\}_{n=1}^N$. This is similar to other reweighting schemes (e.g. (Dieng & Paisley, 2019)), with the most simple one being importance sampling where the proposals are from the prior $p_\theta(z)$, and the weights are normalised density ratios $p_\theta(z, x)/p_\theta(z)$. Importance sampling is an unbiased estimation method, but has huge variance and requires at least exponentially many samples as the KL divergence between the posterior and prior (Chatterjee et al., 2018).

It would then appear that KRR should perform similarly with importance sampling in estimating $\Delta(x)$, but, on closer look, they use slightly different sources of information for estimation. KRR uses a set of samples $(z_n, x_n) \sim p_\theta(z, x)$, whereas importance sampling uses $z_n \sim p_\theta(z)$ and $p_\theta(z, x^*)$. In computing the weights for a particular x^* from the dataset, KRR compares x^* with all sleep samples $\{x_n\}_{n=1}^N$, using a similarity metric determined by the kernel function. The weights α also takes into account of the similarities between all sleep samples. On the other hand, importance sampling uses $p_\theta(z, x^*)$ for a given x^* and computes the weights for each sample of z independently of each other. In addition, the importance sampling weights are constrained to be non-negative and sum up to one, whereas the weights in KRR are not constrained and thus can be more flexible.

B.2. Kernel architecture

In all experiments, we used a squared-exponential kernel $k(x, x') = \exp(-0.5\|\phi_w(x) - \phi_w(x')\|_2^2/\sigma^2)$. The feature ϕ_w can be the identity function, a linear projection, or a linear projection followed by batch normalisation, see Table 1

which lists the architectures used for each experiment. The linear projection and batch normalisation are primarily used on high-dimensional benchmark datasets. Nonlinear projections, such as deep neural networks, did not give significant improvement while consuming more memory. The bandwidth σ is initialised as the median of the distance between $\phi_w(\mathbf{x}^{(n)})$ where $\mathbf{x}^{(n)} \sim p_{\theta_t}(\mathbf{x})$.

C. Experimental details

We list the model and training parameters used to run each experiment in Table 1. The batch size is 100 except for dynamical models and neural process where the batch size is 1.

C.1. Gradient estimation

The toy generative model has $z_1, z_2 \sim \mathcal{N}(0, 1)$, $x|z \sim \mathcal{N}(\text{softplus}(\mathbf{w} \cdot \mathbf{z}) - \|\mathbf{w}\|_2^2, \sigma_2^2)$. The observations are 100 samples for drawn from the model with $w_1 = w_2 = 1$, $\sigma = 0.1$. Note that the ML solution for this synthetic problem is not unique.

For variational learning, the approximate posterior is a factorised Gaussian that minimises the ELBO. The gradient of ELBO was approximated by samples. The mean and variances are initialised as the standard Gaussian and are optimised by Adam with step size 0.01 for 300 iterations, which is sufficient for convergence. For ground truth, we estimated the gradient by importance sampling, with 5×10^4 samples proposed from the prior.

C.2. Spherical prior

The data are 16×16 Gabor images. The orientation is uniformly distributed over one period 0 to π . The generative network is taken from the first two deconvolutional layers of DCGAN so that the output size is 16×16 . For VAE, we used the symmetric convolutional neural network for the encoder and a factorised Gaussian posterior. For \mathcal{S} -VAE, a von Mises-Fisher distribution is used as the posterior.

C.3. Hierarchical models

The penalty assigned to probability vector \mathbf{m} in the categorical distribution is the log pdf of a Dirichlet prior $\log p(\mathbf{q}) = (\alpha - 1) \sum_i \log q_i + \text{const}$, where $q_i = e^{m_i} / \sum_j e^{m_j}$. We use $\alpha = 0.999$. Similarly, for the k 'th component in the mixture, the Normal-InverseWishart distribution has log-likelihood that penalises $\|\mu_k\|$, $\log |\Sigma_k|$ and $\text{Tr}(\Sigma_k^{-1})$. In addition, we also penalise the l_2 norm of neural network weights. These penalisation strengths are set to 10^{-4} .

The relative maximum mean discrepancy (MMD) test (Bounliphone et al., 2016) is used for model comparison based on generated samples. Denote the set of real data by \mathcal{D} and the set of generated samples from model A by \mathcal{D}^A . The null hypothesis for this test is $\text{MMD}(\mathcal{D}, \mathcal{D}^{\text{SIN}}) < \text{MMD}(\mathcal{D}, \mathcal{D}^{\text{ALWS}})$, where MMD is the MMD distance between two sets of samples. The test returns a p -value of 0.514 based on 1500 samples from each of the three distributions, suggesting that the two models perform almost equally well on learning this data distribution. We note that SIN is trained on a full Bayesian version of the model, and the samples are reconstructions given the real dataset, giving an advantage for SIN.

C.4. Parameter identification

The linear basis (weights) are the top 36 independent components of natural images discovered by the FastICA algorithm. Each component is subtracted by their mean and normalised to have unit length. The synthesised dataset is standardised by subtracting the mean and dividing by the standard deviation. The kernel is augmented with an adaptive linear neural network feature with 300 outputs. Using 200 features produces very similar results. The regularisation strength is fixed at $\lambda = 0.001$. Adapting the filters results in slightly different filters as shown in Figure 9.

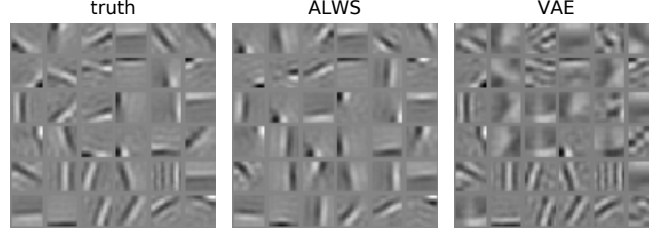
C.5. Neural process

Introduction. We briefly review the neural processes (NPs, Garnelo et al. (2018)). Suppose there is a distribution over function $f \sim \mathcal{P}(f)$, $f : \mathcal{X} \rightarrow \mathcal{Y}$. We observe information a given function f through its potentially noisy values at a set of inputs $(\mathbf{x}, \mathbf{y})|f$. The task is the following: given a set of context pairs $\mathcal{D} := \{(\mathbf{x}_k^C, \mathbf{y}_k^C)\}_{k=1}^K$ drawn from an unobserved function, infer the distribution of the function value at a set of target inputs $\{\mathbf{x}_m^T\}_{m=1}^M$.

NPs represent the posterior of f given \mathcal{C} by a random variable \mathbf{z} , which is combined with \mathbf{x}_m^T to predict the function value.

Experiment	latent dim	data dim	$M(\text{data})$	$N(\text{sleep})$	$L(\text{val})$	λ	# proj	batch norm?	gen lr	grad lr	nepoch
gradient estimation	2	1	100	5 000	—	0.01(f)	—	no	—	—	—
spherical prior	1	256	10 000	2 000	200	0.01	300	no	0.001	0.001	30
pinwheel	2	2	2 500	1 000	200	0.01	—	no	0.001	0.001	2 500
Independent component	36	256	100 000	2 000	200	0.001(f)	300	no	0.001	0.01	100
Matrix factorisation	100	784	5 000	2 000	150	0.001	300	yes	0.001	0.001	300
neural process	50	8	10 000	4 000	200	0.001	—	no	0.0001	0.0001	50
nonlinear oscillation	2/time step	600	1	2 000	200	0.001	200	no	0.001	0.001	5 000
Hodgkin-Huxley	3/time step	1 000	1	2 000	200	0.001	200	no	0.001	0.001	50 000
ecology	1/time step	180	1	2 000	200	0.001	—	no	0.001	0.001	50 000
B-MNIST	16	1 024	60 000	2 000	200	0.1 (f)	300	yes	0.001	0.001	50
MNIST	16	1 024	60 000	2 000	200	0.1 (f)	300	yes	0.001	0.001	50
Fashion	16	1 024	60 000	2 000	200	0.1 (f)	300	yes	0.001	0.001	50
Natural	16	1 024	100 000	2 000	200	0.1 (f)	300	yes	0.001	0.001	50
CIFAR	16	3 072	50 000	2 000	200	0.1 (f)	300	yes	0.001	0.001	50
CelebA	16	3 072	100 000	2 000	200	0.1 (f)	300	yes	0.001	0.001	50

Table 1. Data properties, and model and training parameters of ALWS for each experiment. The regularisation strength λ is sometimes fixed as indicated by (f). See Appendix B.2 for kernel architectures.


 Figure 9. Same as Figure 5 but with λ adaptive.

During training, the training data comprises multiple sets of input-output pairs, and each set is always conditioned on one particular $f \sim \mathcal{P}$. The training data are split into a context set \mathcal{C} , used to condition the representation z , and a target set $\{(\mathbf{x}_m^T, \mathbf{y}_m^T)\}_{m=1}^M$, used to evaluate the likelihood of \mathbf{y}_m^T given z and \mathbf{x}_m^T . Formally, the generative model is specified by

$$\begin{aligned} \mathbf{r} &= \frac{1}{K} \sum_{k=1}^K \rho_{\theta}(\mathbf{x}_k^C, \mathbf{y}_k^C) \\ p_{\theta}(z|\mathbf{r}) &= \mathcal{N}(z|\mu_{\theta}^C(\mathbf{r}), \Sigma_{\theta}^C(\mathbf{r})) \\ p_{\theta}(\{\mathbf{y}_m^T\}|\{\mathbf{x}_m^T\}, z) &= \prod_{m=1}^M \mathcal{N}(\mathbf{y}_m^T|\mu_{\theta}^T(z, \mathbf{x}_m^T), \Sigma_{\theta}^T(z, \mathbf{x}_m^T)). \end{aligned}$$

In short, a latent representation of the context z is drawn from a normal distribution with parameters formed by an exchangeable function of the context set \mathcal{C} , and the likelihood on the target outputs are i.i.d. Gaussian conditioned on z and \mathbf{x}_m^T . The objective for learning is to maximise the likelihood of the target output conditioned on the corresponding context set from the same underlying f and the target input. Once trained, the neural process is able to produce samples from the distribution of function values (target outputs) at context inputs.

The encoding function ρ_{θ} plays the role of an inferential model, but we can view it as a function that parametrises the “prior” distribution on z given the context set, and the parameters in ρ can be regarded as belonging to the generative model. The gradient model trained by KRR also needs to be conditioned on each context set, but for simplicity, we train a gradient model for a single context followed by θ update. Garnelo et al. (2018) trained the neural processes by maximising an ELBO with posteriors of the form

$$q(z|\mathcal{C}, \mathcal{T}) = p_{\theta}(z|\mathbf{r}^{CT}), \quad \mathbf{r}^{CT} = \frac{1}{K} \sum_{k=1}^K \rho_{\theta}(\mathbf{x}_k^C, \mathbf{y}_k^C) + \frac{1}{M} \sum_{m=1}^M \rho_{\theta}(\mathbf{x}_m^T, \mathbf{y}_m^T),$$

which is an approximation.

Experiments. We train a neural process on a $\mathcal{P}(f)$ that have samples as shown in Figure 10 (top). They are sinusoids with random amplitudes and phase shifts and supported on $[-\pi, \pi]$. The observations are contaminated with Gaussian noise with standard deviation 0.1. Conditioning the function with a context input around $-\pi$, 0.0 and π induces large uncertainty over f ; thus, we can use this to probe the representation of uncertainty.

In the NP model, the representation \mathbf{r} and z are both 50-dimensional. And the encoding and decoding networks are fully connected with ReLU nonlinearities. During training, the number of context pairs $K = 4$, and the target set contains the context pairs and an additional four pairs, so $M = 8$ and $\mathcal{C} \subset \mathcal{T}$. The gradient model is trained for each given context set, and hence the batch size is 1. A small learning rate of 0.0001 is used for all models and parameters. The gradient model is trained to take sleep samples \mathbf{y}_m^T evaluated for this single \mathcal{C} at each \mathbf{x}_m^T . The kernel takes $\{\mathbf{y}_m\}_{m=1}^8$ as a single vector. We note that other kernels on sets could be used.

During test time, we evaluate the predicted function value of a dense grid of points in $[-\pi, \pi]$ given 1 to 4 context pairs. As shown in Figure 10 (lower panels), when the number of context points is small, the model trained with ALWS makes more accurate predictions, and better reflects the uncertainty of the function value when the context set is uninformative. Given four context pairs (as in training), we test the learned model on 500 functions from $\mathcal{P}(f)$ and evaluate how close samples of $\mathcal{P}(f|\mathcal{C}, \mathbf{x}_m^T)$ are to the true function at $M = 100$ target locations. We use either the posterior mean or a random

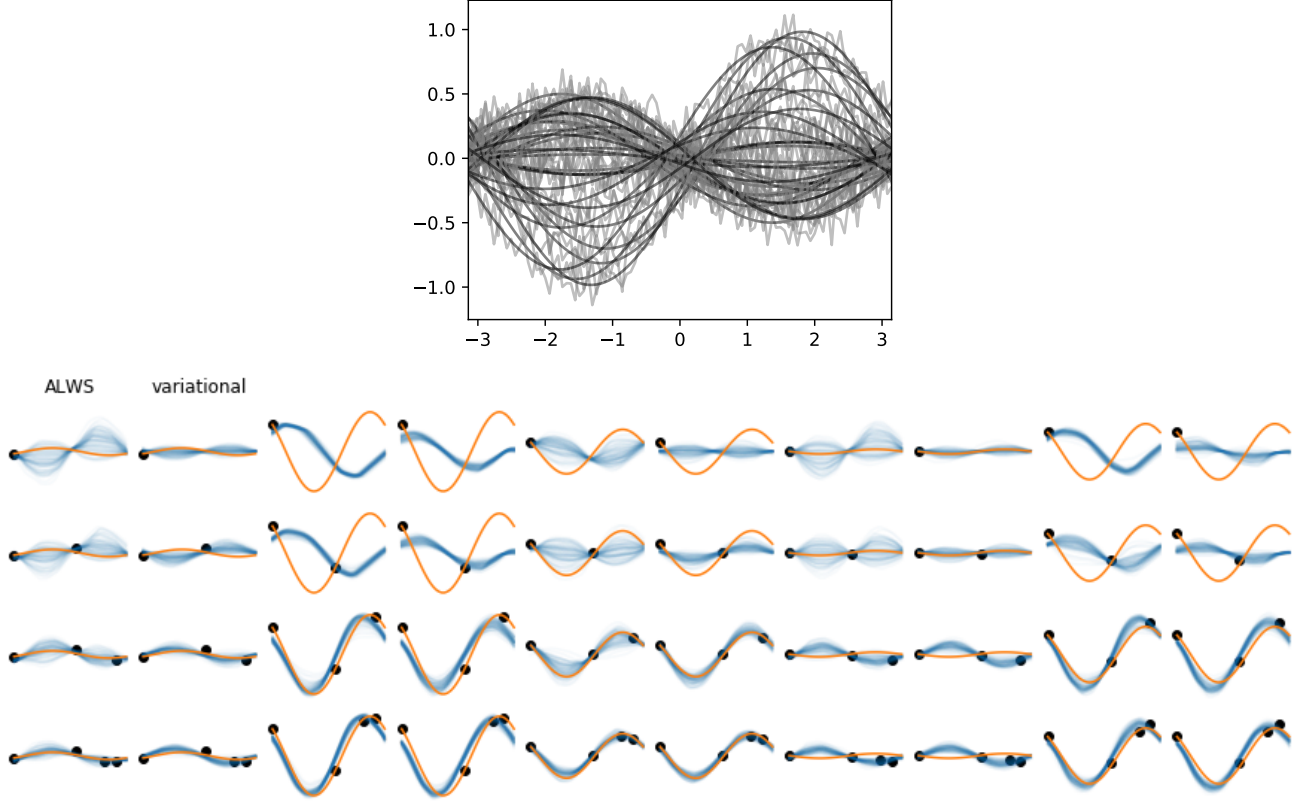


Figure 10. Neural processes. Top: samples from prior distribution of functions. Black: Latent function. Grey: noisy observations. Bottom: posterior samples (blue lines) from ALWS (odd columns) and the original variational method (even columns). Orange lines are true latent functions f . Black dots are context pairs.

posterior sample from the posterior as a point estimate, and measure the performance by mean squared error. We find that the errors are significantly smaller for ALWS-trained model based on paired tests for the posterior mean prediction (paired t-test, $t = -3.47, p = 0.00056$; mean of ALWS, -5.11; variational, -4.99. Wilcoxon test, $W = 44837.0, p = 3.7 \times 10^{-8}$, median of ALWS, -5.11, variational, -4.98) and the random sample prediction (paired t-test, $t = -2.09, p = 0.037$; mean of ALWS, -4.87; variational, -4.77. Wilcoxon test, $W = 53762.0, p = 0.0061$, median of ALWS, -4.91, variational, -4.69).

C.6. Nonlinear dynamic model

We run ALWS for generative models whose priors are defined through nonlinear transitions in time. In all of the experiments, we treat each sequence as a single multi-dimensional data point.

C.6.1. NONLINEAR OSCILLATIONS

We generate data from a nonlinear oscillation process according to the following equations used by [Wenliang & Sahani \(2019\)](#)

$$\mathbf{z}_t = \text{Rot}(\mathbf{z}_{t-1}) + \epsilon_t^{(z)}, \quad \mathbf{x}_t = \text{Img}(\mathbf{z}_{t,1}) + \epsilon_t^{(x)}$$

$$\text{Rot}(\mathbf{z}_t) = \mathbf{R}_\alpha \mathbf{z}_t \frac{r(\|\mathbf{z}_t\|_2)}{\|\mathbf{z}_t\|_2}, \quad r(a) = \text{sigmoid}(4(a - 0.3)), \quad [\text{Img}(z)]_i = \exp(-0.5(z - \bar{z}_i)^2 / 0.3^2)$$

where \mathbf{R}_α is a rotation matrix by α radians, Img maps one of the latent dimensions into a 20-pixel image through Gaussian bumps with evenly spaced centers at $\bar{z}_i, i \in \{1, \dots, 20\}$. Intuitively, the latent \mathbf{z} is rotated by α and scaled radially so that its length remains close to 1. Samples of \mathbf{x}_t for all $t \in \{1, \dots, T\}$ can be plotted side by side as a $20 \times T$ image, which is shown in Figure 11 (top).

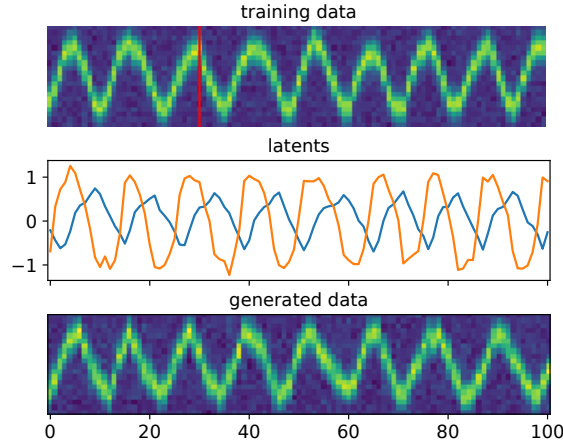


Figure 11. Nonlinear oscillations. Top: an example trajectory. Only the first 30 time steps marked by the red line is used for training. Three such 30 time step traces are used for training. Middle: latent space learned by ALWS. Bottom: Generated trajectory.

We train the following generative model:

$$p_{\theta}(z_t|z_{t-1}) = \mathcal{N}(z_t; \text{NN}_w^{(z)}(z_{t-1}), \Sigma_z), \quad p_{\theta}(x_t|z_t) = \mathcal{N}(x_t; \text{NN}_w^{(x)}(z_t), \Sigma_x),$$

where the parameters are the weights and biases in the neural networks (NN), and the diagonal covariance matrices $\Sigma_{(\cdot)}$'s. The number of units are fully connected with $2 \rightarrow 20 \rightarrow 2$ neurons for $\text{NN}^{(z)}$ and $2 \rightarrow 20 \rightarrow 20$ for $\text{NN}^{(x)}$. The tanh is used as the nonlinearity. We train the model on a single sequence of 30 time steps and then generate a 100-step sequence of the learnt latents and observations shown in Figure 11. The latents correctly capture the position, which directly sets the data, and the velocity, which needs to be learned from data.

C.6.2. HODGKIN-HUXLEY (HH) EQUATIONS

The HH equations are described by

$$C_m \dot{V}(t) = -g_l[V(t) - E_l] - \bar{g}_N m^3(t) h(t)[V(t) - E_N] - \bar{g}_K n^4(t)[V(t) - E_K] + I_{\text{in}}(t) + \epsilon(t) \\ \dot{e}(t) = \alpha_e(V(t))[1 - e(t)] - \beta_e(V(t))e(t), \quad e \in \{m, h, n\}$$

where α_e and β_e are nonlinear functions of $V(t)$ involving a parameter V_T that sets the threshold for action potentials, see (Pospischil et al., 2008) for details.

We used forward-Euler method for simulation with a time step of $\Delta t = 0.05 \text{ ms}$. At each step of the simulation, we add a small Gaussian noise of standard deviation $\sigma_z = 0.1 \text{ mV}$ to V_t as process noise. The measurements noise added to observations (but not propagated to V_{t+1}) is Gaussian with standard deviation 1.0 mV . There 10 parameters for the resulting discrete-time state-space model: $\theta = \{C_m, g_l, E_l, \bar{g}_N, E_N, \bar{g}_K, E_K, V_t, \sigma_z, \sigma_x\}$.

We train and test the model under different input current sequences I_{in} . The results are shown in Figure 12. We simulate a single trajectory from the model with some true parameters and a noisy current injection shown in Figure 12(1st row). This sequence is used as the training data Figure 12(2nd row, dotted). We then perturb these parameters, making the simulated trajectories unrealistic Figure 12(3rd row). After training, the simulated trajectories look almost identical to the training data Figure 12(2nd row, solid). To test whether the learned model can be used for prediction under a different current injection, we simulate trajectories given an unseen test current Figure 12(4th row). The responses of membrane potential under true parameters are shown in Figure 12(5th row). Samples from the trained model Figure 12(6th row, solid) under this unseen current are very similar to the trajectories given real parameters, showing generally correct phase, periodicity and amplitude. The simulated responses have less variation between trajectories, which could be due to training under a single sequence. Indeed, not all parameters converge to the true parameters Figure 12 (bottom panels).

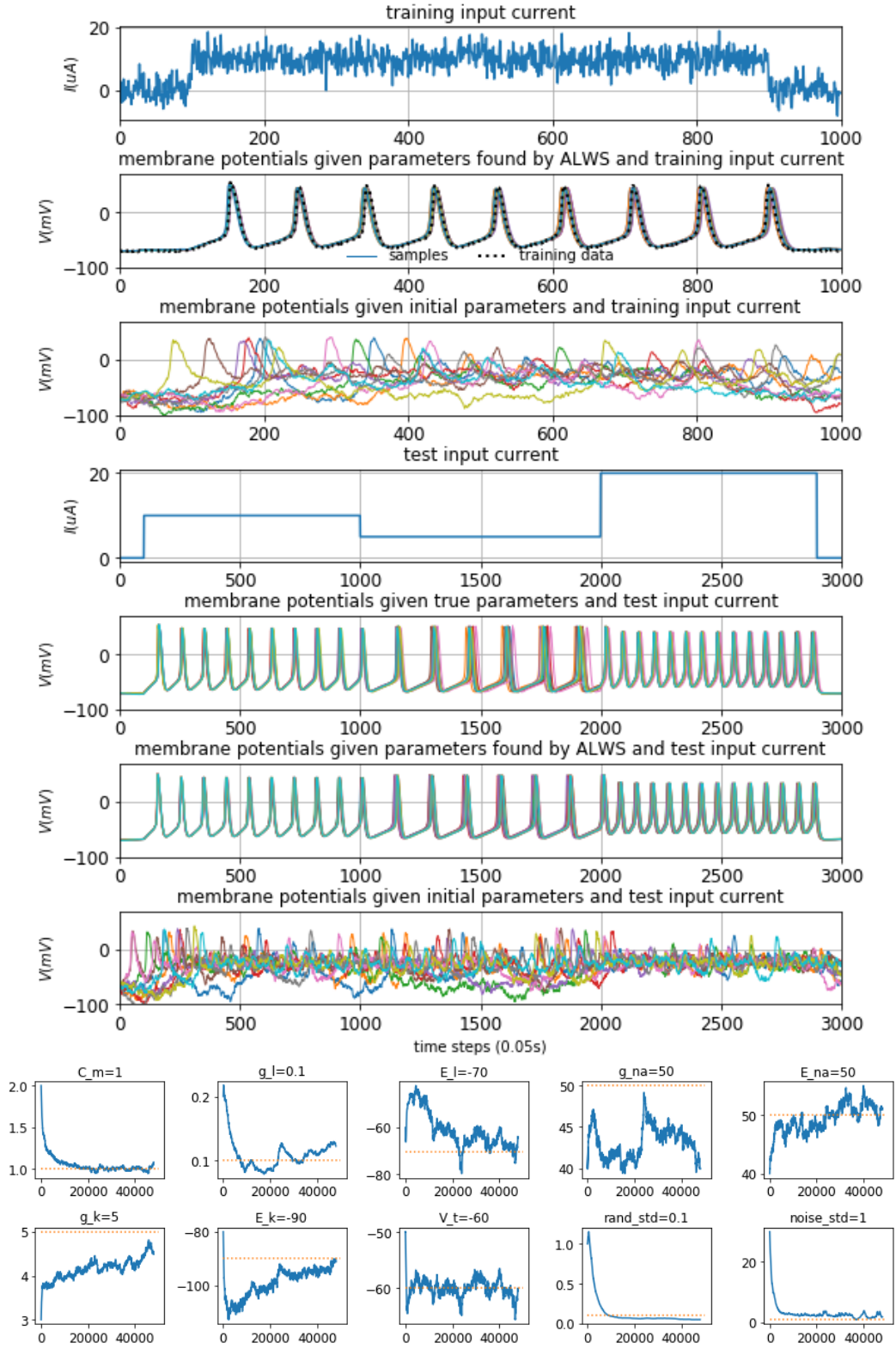


Figure 12. Hodgkin Huxley simulations. Top seven panels: 1st row, input current I_{in} during training. 2nd-3rd rows, trajectories given learnt and initial parameters under training input current. 4th row, test input current. 5th-7rd rows, trajectories given true, learnt and initial parameters under test input current. Bottom 10 panels: Blue solid: parameter value at each iteration. Yellow dashed: true parameter values.

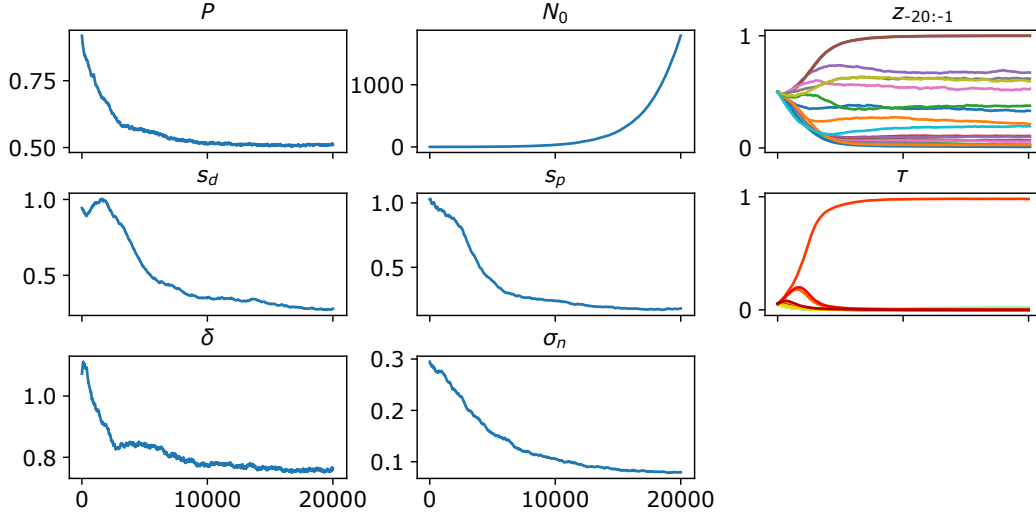


Figure 13. Evolution of parameters in the ecological model for blowfly population.

C.6.3. ECOLOGICAL DATA

We train a model that describes the evolution of blowfly population size under food limitation (Wood, 2010). The model is given by

$$\begin{aligned} \tau &\sim \text{Categorical}(\mathbf{m}), \tau \in \{1, \dots, 20\}, \quad e_t \sim \text{Gamma}\left(\frac{1}{\sigma_p^2}, \sigma_p^2\right), \quad \epsilon_t \sim \text{Gamma}\left(\frac{1}{\sigma_d^2}, \sigma_d^2\right), \\ z_t &= P x_{t-\tau} \exp\left(-\frac{x_{t-\tau}}{N_0}\right) + x_t \exp(-\delta \epsilon_t), \quad p(x_t | z_t) = \text{LogNormal}(\log(z_t), \sigma_n^2) \end{aligned}$$

Note that τ is a discrete delay drawn from a categorical distribution with logit parameters \mathbf{m} , e_t and ϵ_t are stochastic variations in births and deaths following Gamma distribution with a common mean 1.0 and standard deviations σ_p^2 and σ_d^2 , respectively. The observation is noisy with log-normal noise so that x_t remains positive. Observations in the first 20 time steps depend on some past data that is not observed, so we modelled these past data $x_{-20:-1}$ as parameters, which are constrained to be between 0 and 1.0. Thus, this model has parameters $\theta = \{\mathbf{m}, \sigma_d, \sigma_p, P, N_0, \delta, \sigma_n, x_{-20:-1}\}$

We fit the model on a data sequence of length 180, normalised to be between 0 and 1.0. The evolution of parameters is shown in Figure 13. As our training objective is different from that of ABC methods, we do not make direct quantitative comparison with them. But compared with the samples from three ABC methods shown in (Park et al., 2016) (Figure 2B), it is clear that samples from ALWS are visually more similar to the training data.

C.7. Sample quality on benchmark datasets

C.7.1. DATA PROCESSING

All images have 32×32 pixels by their original sizes (Natural, CIFAR-10), or by zero-padding (MNIST, F-MNIST) or interpolation (CelebA). The binarised MNIST is statically binarised once before training. Each pixel is set to 1 with probability equal to the pixel value after rescaling to between 0 and 1. The natural images⁹ are patches from large natural scenes. No clipping is applied. Original MNIST Fashion MNIST, CIFAR-10 and CelebA images are rescaled to between -1.0 and 1.0.

C.7.2. MODEL AND TRAINING DETAILS

All methods use the same neural network as the DCGAN without the last convolutional layer to make the image size 32. Batch size is 100 for each update of generative and gradient model parameters. We run each algorithm on each dataset with 10 different initialisations. The neural network in the generative model has ReLU nonlinearities in intermediate layers. The

⁹github.com/hunse/vanhateren

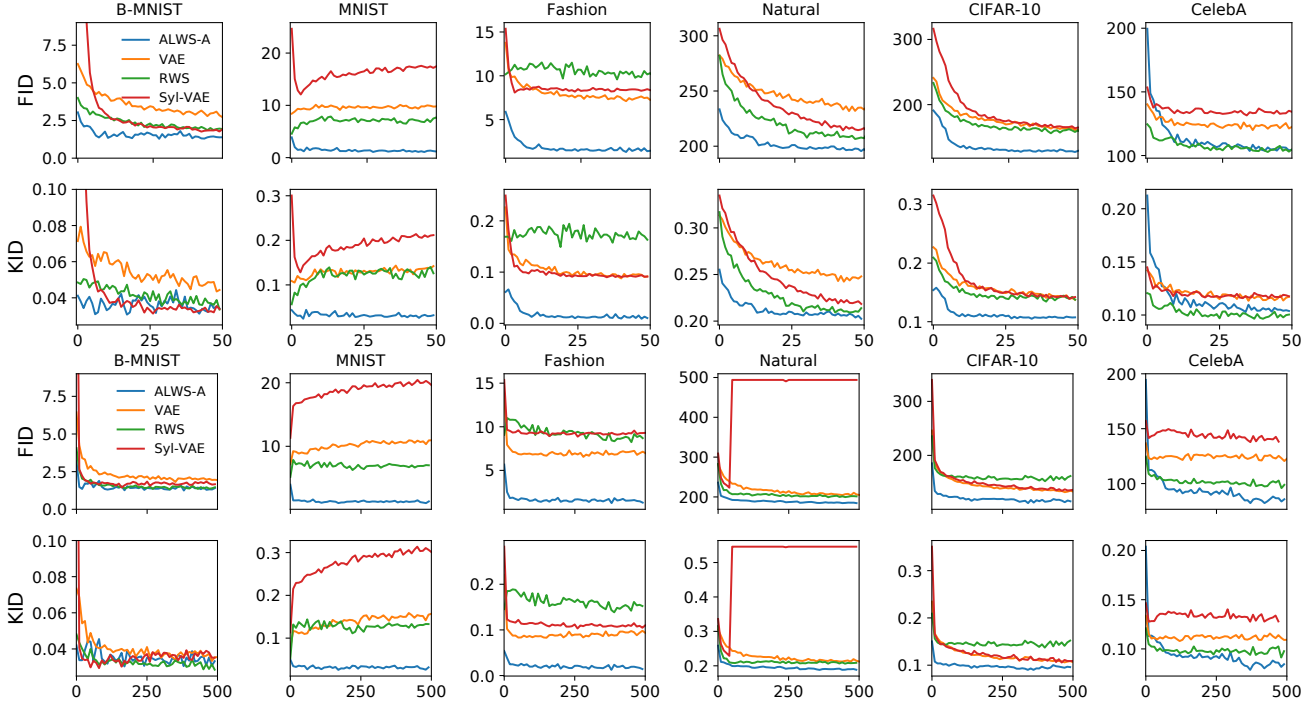


Figure 14. KID and FID scores at the end of each epoch for selected algorithms on convolutional architecture. Top two rows show distances during a run of 50 iterations at every iteration, and the bottom two rows show another run of 500 iterations at every 10th iteration.

nonlinearity for the final layer depends on the dataset: it is sigmoid for binary MNIST, linear natural images, and tanh for the other datasets.

All methods are trained for 50 epochs except for SIVI which was trained for 1 000 epochs. The optimizer is Adam with a fixed learning rate of 0.001. For ALWS, we use 2 000 sleep samples for training the gradient model. The kernel is augmented by the linear projection to 300 dimensions for all datasets. A larger number of output dimension produced better results but induces longer run time. The weights of the projection are updated after the first five epochs. The regularisation parameter λ is fixed at 0.1; this helps sample quality for CIFAR and CelebA, but does not affect or worsens sample quality for the other datasets. For ALWS-F, a fixed random projection is used throughout training. For ALWS-A, the linear weights are training at each parameter update after five epochs, using the two-stage training.

For VAE, the encoder network is symmetrical to the generative network and is appended with a final linear layer for posterior statistics.

For Syl-VAE. We change the gated convolutional layer in the decoder network to the same network as all the other methods. Other parts of the model remain the same. We use the orthogonal flow. A lower learning rate of 0.0005 is used for stability.

For SIVI, we find the model is unstable for learning rate of 0.001, so we change it to 0.0001. It also takes more epochs to produce good samples, so we train for 1000 epochs. We use $J = 10$ proposals from the Gaussian posterior.

For RWS, each parameter update is accompanied with both wake and sleep updates of the encoder parameters, using $K = 50$ proposals. A larger K can cause lower signal-to-noise ratio of the update for the encoder network.

For WGAN-GP, learning is unstable for a learning rate of 0.001, so we train the model using a learning rate of 0.0001 for 50 epochs, which was not sufficient for it to produce good images. We also run WGAN-GP for 500 epochs on all datasets and show the results of WGAN-GP just for reference, as it is not trained using the maximum likelihood objective.

To evaluate the quality, we use standard metrics FID and KID, which are computed using features of penultimate layers of neural networks pre-trained on relevant datasets. For both MNISTs, the features are from the LeNet trained to classify MNIST digits. For Fashion, we used the LeNet network trained to classify the objects. For Natural, CIFAR-10 and CelebA,

we use inception network trained on ImageNet classification. For Natural, we duplicate the image along the channel axis to fill the three colour channels.

ALWS-A has lower FID and KID than other maximum likelihood methods in most cases, especially on original MNIST and Fashion MNIST, but does not reach the level of WGAN-GP.

The KID and FID values during training are shown in Figure 14. ALWS performs consistently better at every training epoch on all datasets except B-MNIST. On MNIST, ALWS-A converged the fastest and generates samples with stable quality. On CIFAR, ALWS-A and RWS converged faster than the others, but VAE and Syl-VAE converge very slowly. We note that these figures are plotted against epochs, not wall-clock time. The run time of ALWS is much longer than the other methods, taking around 3.5 seconds per iteration on a GeForce 1080 GPU, or 2.5 seconds on a Quadro P5000 with kernel adaptation. Nonetheless, this cost is worth the improvement over other maximum likelihood methods.

The samples from all methods are shown in Figure 15 to Figure 20. These include samples from models presented in the main text, the WGAN-GP for 500 epochs, and the AL-P algorithm introduced in Appendix B.1.2.

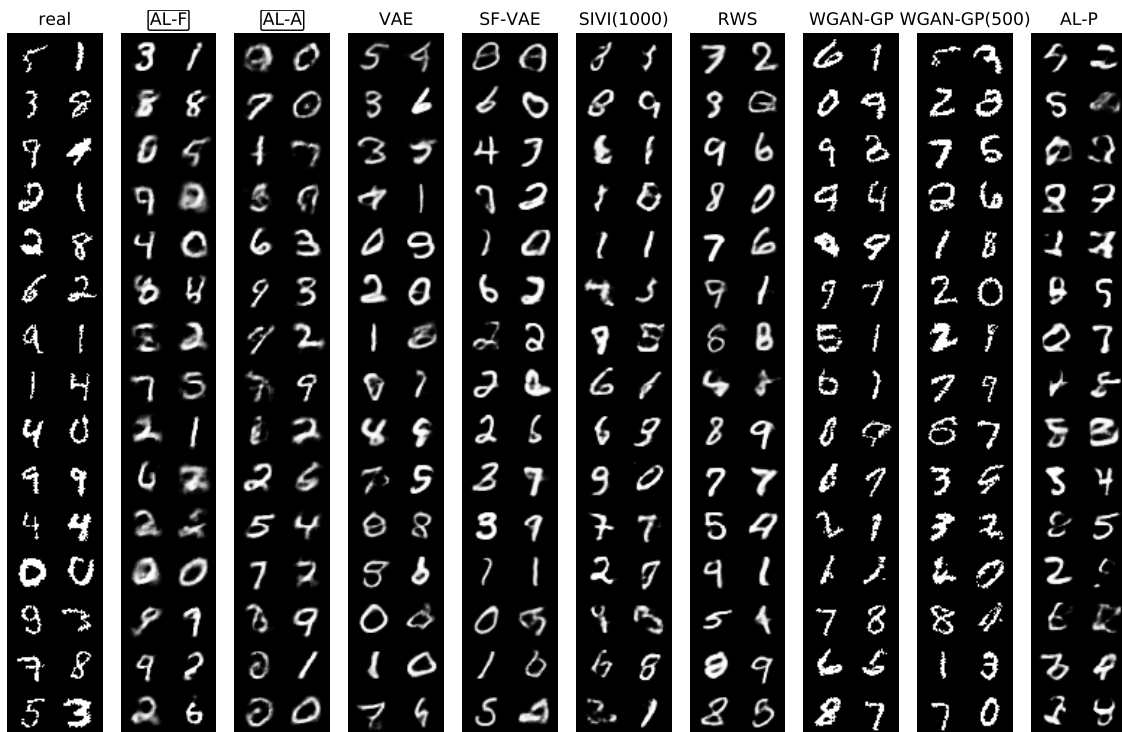


Figure 15. Samples for B-MNIST. Our main algorithms presented in the main text are highlighted in box. Each model is trained for 50 epochs, except otherwise indicated in parenthesis next to algorithm name.



Figure 16. Samples for MNIST. Our main algorithm is highlighted in box. Each model is trained for 50 epochs, except otherwise indicated in parenthesis next to algorithm name.



Figure 17. Samples for Fashion. Our main algorithms presented in the main text are highlighted in box. Each model is trained for 50 epochs, except otherwise indicated in parenthesis next to algorithm name.

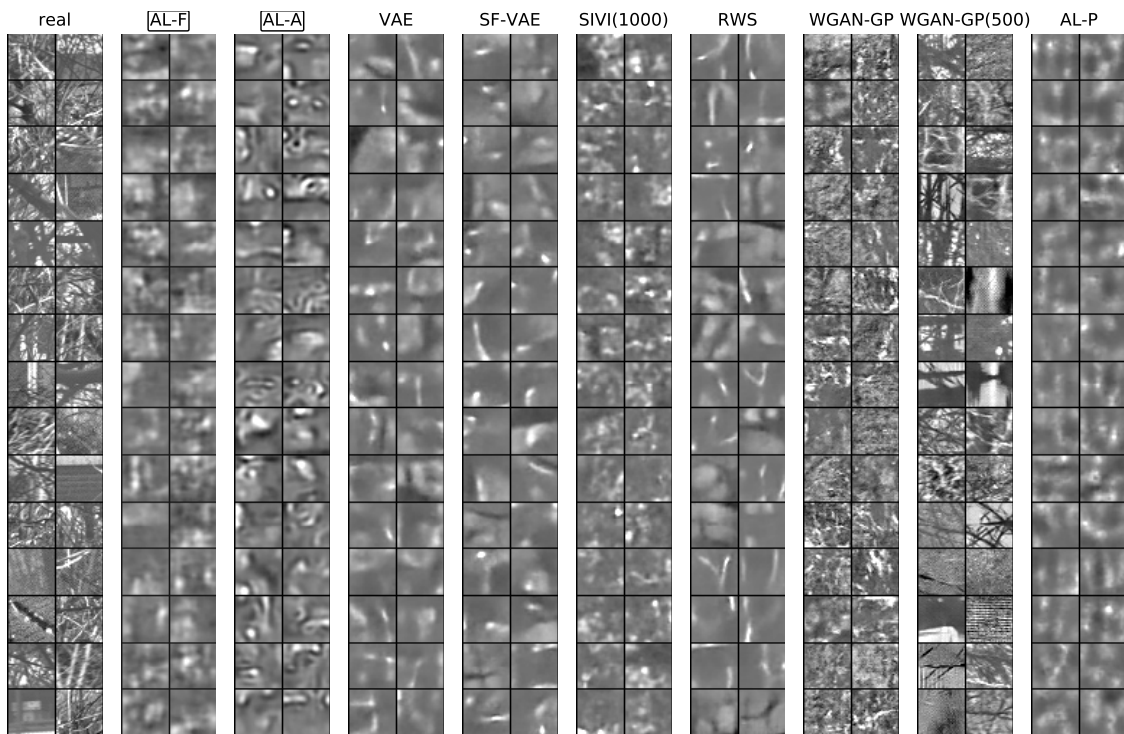


Figure 18. Samples for Natural. Our main algorithm is highlighted in box. Each model is trained for 50 epochs, except otherwise indicated in parenthesis next to algorithm name.

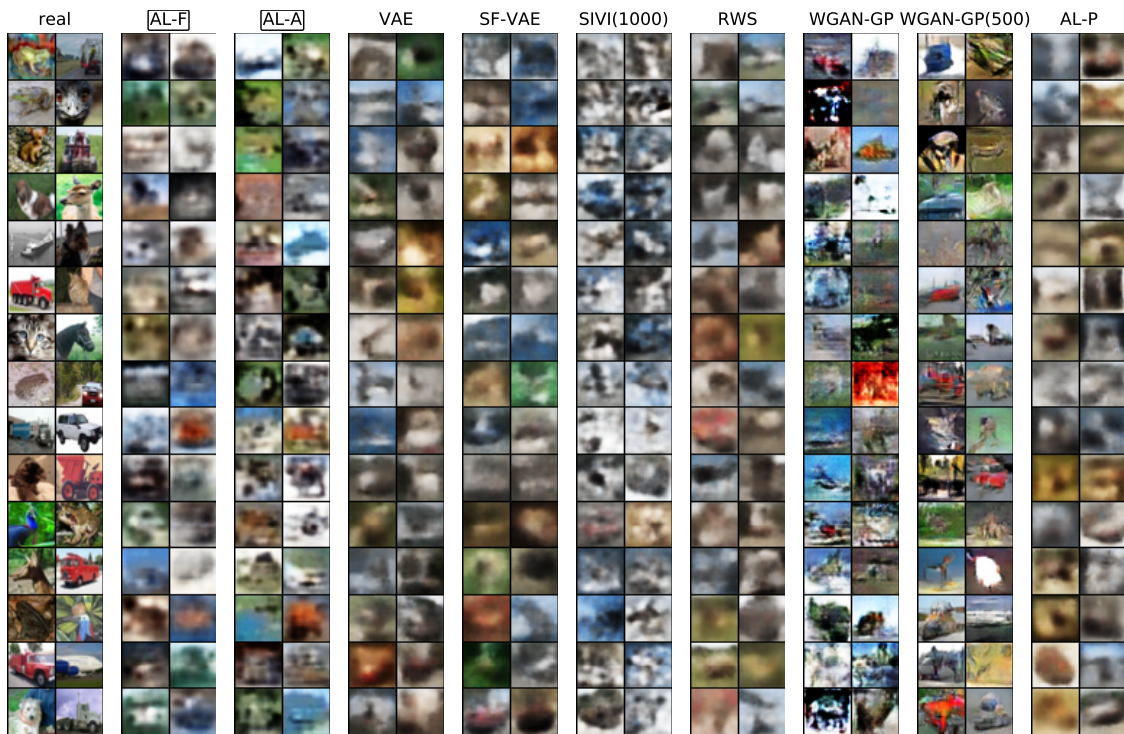


Figure 19. Samples for CIFAR-10. Our main algorithms presented in the main text are highlighted in box. Each model is trained for 50 epochs, except otherwise indicated in parenthesis next to algorithm name.

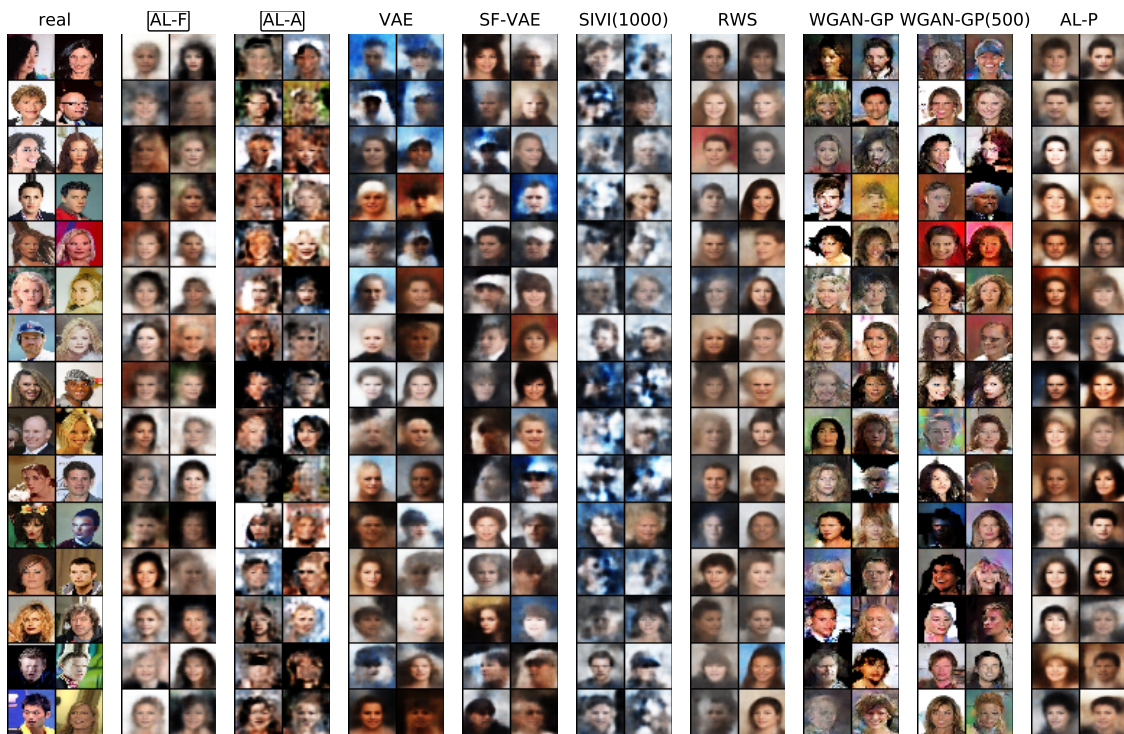


Figure 20. Samples for CelebA. Our main algorithms presented in the main text are highlighted in box. Each model is trained for 50 epochs, except otherwise indicated in parenthesis next to algorithm name.

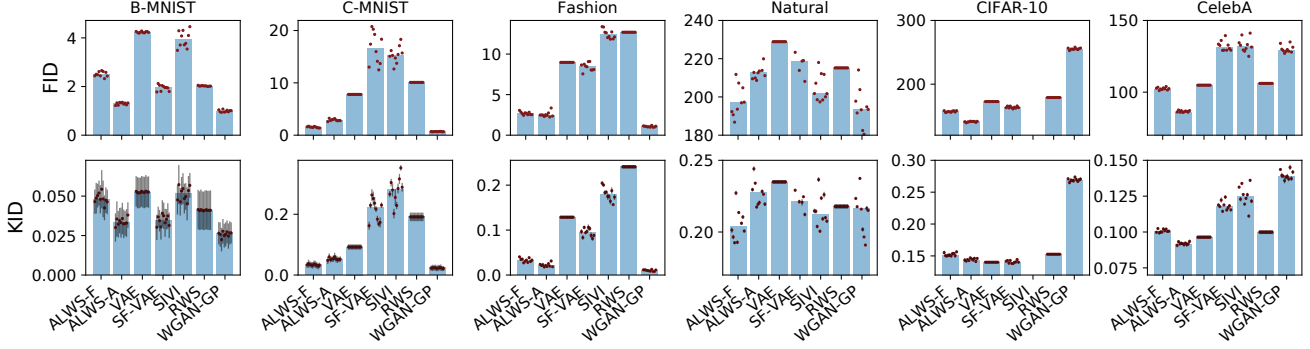


Figure 21. Same as Figure 21 but using fully connected networks. None of the SIVI runs on CIFAR-10 converge.

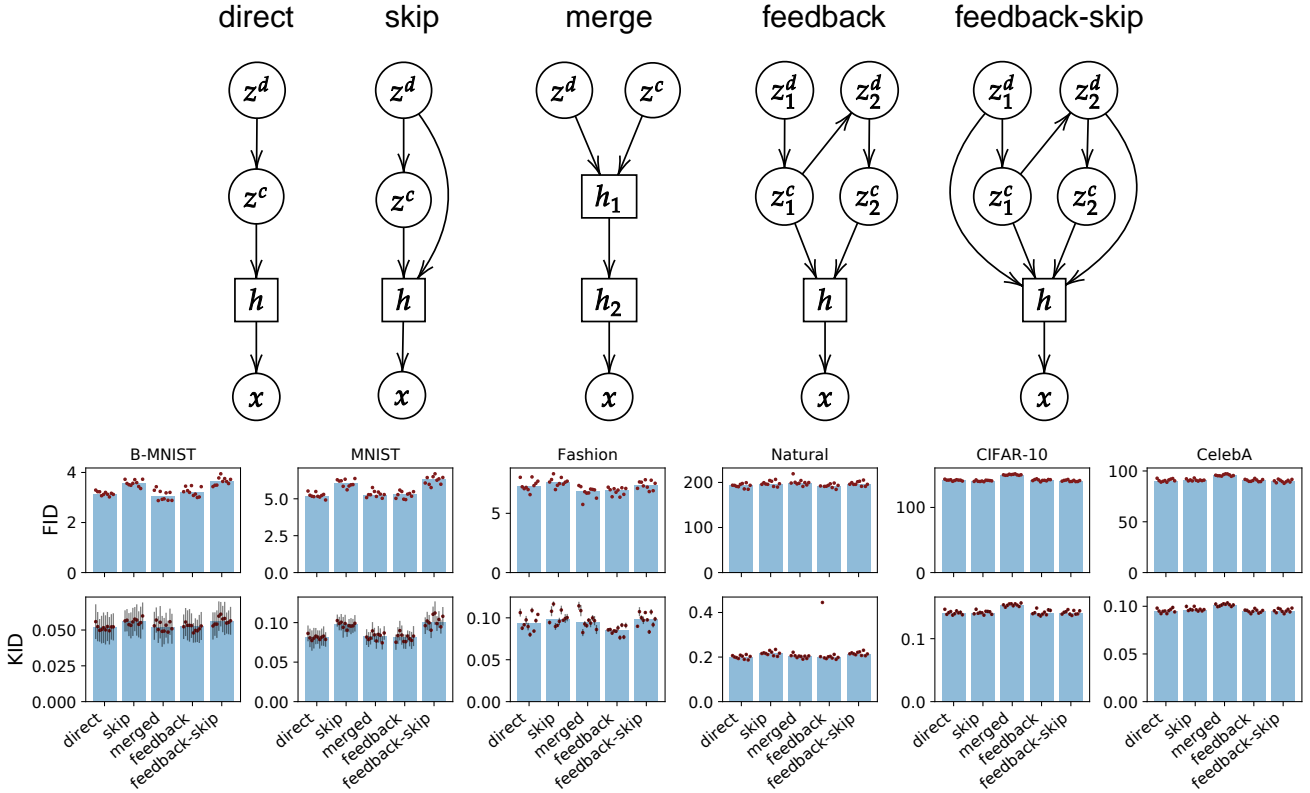


Figure 22. Top, the graphical representations of the generative models. Circles indicate random variables, with z^d as discrete Bernoulli and z^c as continuous Gaussian. Squares indicate deterministic nodes that are ReLU neurons activated by nodes with incoming arrows. The dimensionality of z^d is 10, z^c is 16, z_1^d and z_2^d are 5, and z_1^c and z_2^c are 8. The node h has 512 neurons. Bottom, FID and KID scores of generated images from architecturally complex models

C.7.3. RESULTS ON FULLY CONNECTED NETWORKS

We repeat the experiments for fully connected layers, with architecture $16 \rightarrow 512 \rightarrow 512 \rightarrow \text{image dimension}$. The results are shown in Figure 21. According to FID, models trained by ALWS out-perform other ML methods on all datasets except Natural. KID agrees with FID except on CIFAR-10 where KID values are roughly the same for all ML methods.

C.7.4. RESULTS ON COMPLEX GENERATIVE NETWORKS

The goal here is to test how model architecture affects the quality of the generated samples. Discrete variables can be used to capture features such as object category, so including these in the generative model may be beneficial. In order to train models with discrete latent variables, explicit reparameterisation schemes have been developed in the past by continuous relaxation or overlapping transformation (Jang et al., 2017; Vahdat et al., 2018; Rolfe, 2017), and has shown differential performances. On the other hand, amortised learning is agnostic to the discrete or continuous nature of the latents.

We set out to explore different architectures while fixing the number of Bernoulli and Gaussian latent variables, respectively, and keep the number of parameters roughly the same. The different graphs are depicted in Figure 22 (top) and described in the legend. The **direct** model is a simple chain graph. The top Bernoulli layer connects to a Gaussian layer, where the mean is a function of the Bernoulli, and the variance is fixed at 1.0. The **skip** model is similar to the direct model, except that it adds an additional connection from the discrete latents to the hidden units in the network. The **merged** model combines the Bernoulli and Gaussian latents at the top layer, which goes through a first hidden h_1 layer of 16 units before feeding into the wide h_2 layer. The **feedback** model has an architecture inspired by (Vahdat et al., 2018). The latent z_1^c parametrises the logits for z_2^d . The **feedback-skip** model is based on **feedback** and adds a skip connection to h from the top Bernoulli layer.

The results are shown in Figure 22 (bottom). Interestingly, we did not find any strong effect of model architecture on FID or KID. But the direct, merged and feedback architectures are clearly better than the other two for the two MNIST datasets according to FID.